https://ntrs.nasa.gov/search.jsp?R=19740015210 2020-03-23T08:30:16+00:00Z

(NASA-TM-X-70076) THE EFFECT OF GRAIN BOUNDARIES ON THE RESISTIVITY OF POLYCRYSTALLINE SILICON Ph.D. Thesis - Va. Univ. (NASA) 122 p HC $9.25 CSCL 20L G3/26
N74-23323
Unclas 38480

# The Effect of Grain Boundaries on the Resistivity of Polycrystalline Silicon

---

A Dissertation

Presented to

the Faculty of the School of Engineering and Applied Science

University of Virginia

---

In Partial Fulfillment

of the Requirements for the Degree

Doctor of Philosophy (Materials Science)

by

Archibald L. Fripp, Jr.

May 1974

Reproduced by
NATIONAL TECHNICAL
INFORMATION SERVICE
US Department of Commerce
Springfield, VA. 22151

APPROVAL SHEET

This dissertation is submitted in partial fullfillment of the requirements for the degree of Doctor of Philosophy (Materials Science)

Author

Approved:

Faculty Adviser

Dean, School of Engineering and Applied Science

May 1974

Acknowledgments

The author wishes to gratefully acknowledge the following for their invaluable aid in making this dissertation possible:

The National Aeronautics and Space Administration for sponsoring the research reported herein;

Dr. William A. Jesser, of the University of Virginia, for his patience, guidance, and encouragement;

Dr. Robert L. Stermer for suggesting the problem area;

My management, especially Mr. Charles Husson, and fellow workers of the Flight Instrumentation Division, for the opportunity to work, encouragement to finish, and patience with my impatience;

Messrs. Harry F. Benz and John J. Wells for helpful discussions and computer programming aid;

Miss Freda Richardson, Mrs. Joanne Halvorson, and Mr. Charles R. Pruitt for help in preparing the manuscript;

and last but certainly not least;

Jean, Jon, and Mike - who made it all worth while.

ii-a

# Table of Contents

| Chapter | | Page |
|---|---|---|
| I. | Introduction | 1 |
| II. | Literature Review | 3 |
| III. | Experimental Procedure | 26 |
| IV. | Experimental Results | 41 |
| V. | Discussion | 71 |
| VI. | Summary | 102 |
| References | | 105 |

List of Tables

Table Page

I. Resistivity vs. Doping Level in Amorphous Silicon (ref. 28) . . . . . . . . . . . . . . 7

II. Reported Properties on Amorphous Silicon. . . . 9

III. Silicon Microstructure vs. Doping Level (ref. 43) . . . . . . . . . . . . . . . . . . . 13

IV. Electrical Properties of Polycrystalline Silicon (ref. 37) . . . . . . . . . . . . . . . 15

V. Electrical Properties of Polycrystalline Silicon (ref. 45 and 47). . . . . . . . . . . . 16

VI. Electrical Properties of Polycrystalline Silicon (ref. 49) . . . . . . . . . . . . . . . 19

VII. Electrical Properties of Polycrystalline Silicon (ref. 43) . . . . . . . . . . . . . . . 21

VIII. Reported Properties of Polycrystalline Silicon . . . . . . . . . . . . . . . . . . . . 23

IX. Cleaning Procedure for Silicon Wafers . . . . . 27

X. Oxidation Procedure . . . . . . . . . . . . . . . 27

XI. Flow Rates of Gases Used in Depositing Silicon 30

XII. Standard Growth Conditions. . . . . . . . . . . 41

XIII. Resistivity of Phosphorous Doped Silicon Films . . . . . . . . . . . . . . . . . . . . . 44

XIV. Resistivity of Boron Doped Silicon Films. . . . 46

| Table | | Page |
|---|---|---|
| XV. | Resistivity of Silicon Films - High Temperature Deposition . . . . . . . . . . . . . | 49 |
| XVI. | Resistivity of Silicon Films - Thickness Dependence . . . . . . . . . . . . . . | 51 |
| XVII. | Resistivity of Silicon Films After Oxidation . . | 56 |
| XVIII. | Resistivity of Silicon Film After Repeated Oxidation. . . . . . . . . . . . . . . . . . . . | 58 |
| XIX. | Acceptable Values of G . . . . . . . . . . . . . . | 88 |

# List of Figures

Figure — Page

1. Silicon Oxidation System . . . . . . . . . . . . 28
2. Silicon Deposition System. . . . . . . . . . . . 31
3. Four Point Probe System. . . . . . . . . . . . 36
4. Measurement of Film Thickness. . . . . . . . . 37
5. Resistivity of Silicon Films vs. Phosphous Doping Level . . . . . . . . . . . . . . . . . 45
6. Resistivity of Silicon Films vs. Boron Doping Level . . . . . . . . . . . . . . . . . 47
7. Resistivity of Silicon Film vs. Phosphous Doping Level . . . . . . . . . . . . . . . . . 50
8. Resistivity of Silicon Films vs. Thickness, High Doping. . . . . . . . . . . . . . . . . 52
9. Resistivity of Silicon Films vs. Thickness, Moderate Doping. . . . . . . . . . . . . . . 53
10. Resistivity of Silicon Films After Oxidation. . . . . . . . . . . . . . . . . . 57
11. Change in Resistivity After Oxidation. . . . . 59
12. Change in Resistivity After Repeated Oxidations . . . . . . . . . . . . . . . . . 60
13. Transmission Electron Photomicrograph of Silicon Film. . . . . . . . . . . . . . . 62
14. Transmission Electron Diffraction Pattern . . . . . . . . . . . . . . . . . . 62

Figure Page

15. Lapped and Oxidized, Large Grain Film . . . . . . . 64

16. Composite Figure Showing Microstructures vs. Film Thickness . . . . . . . . . . . . . . . 65

17. Continuous and Non Continuous Films . . . . . . . . 66

18. Composite of Resistivity Data . . . . . . . . . . . 68

19. Resistivity of Silicon Films Before and After Anneal. . . . . . . . . . . . . . . . . . 69

20. Nonhomogeneous Conductor-Perpendicular Layers . . 79

21. Nonhomogeneous Conductor-Parallel Layers. . . . . 79

22. Nonhomogeneous Conductor-Perpendicular and Parallel Layers . . . . . . . . . . . . . . . . 80

23. Sensitivity of Apparent Resistivity for Different G . . . . . . . . . . . . . . . . . . . 89

24. S vs. Dopant Level with Fixed G . . . . . . . . . . 97

# List of Symbols

| | |
|---|---|
| $A$ | cross sectional area |
| $A_{gb}$ | grain boundary area per unit volume |
| $D$ | diffusion coefficient |
| $e$ | magnitude of electron charge |
| $\varepsilon_g$ | grain boundary surface energy |
| $\varepsilon_s$ | surface energy |
| $G$ | grain boundary conductivity divided by electron charge |
| $I$ | current |
| $\ell$ | length of conductor layer |
| $\ell_{gb}$ | thickness of grain boundary region |
| $\ell_s$ | grain diameter |
| $n$ | electronic conduction |
| $N$ | dopant atom concentration |
| $N$ | number of conductor layers |
| $N_a$ | concentrations of acceptor atoms |
| $N_b$ | density of excess bonds |
| $N_d$ | concentration of donor atoms |
| $n_e$ | density of conduction electrons |
| $N_g$ | density of dopant atoms in grain boundary region |
| $n_{gb}$ | density of charge carriers in grain boundary region |
| $n_h$ | density of conducting holes |
| $n_i$ | intrinsic charge carrier concentration |

| | |
|---|---|
| $n_s$ | charge carrier concentration in a silicon crystal |
| $n_s$ | charge carrier concentration in a crystalline grain |
| $N_s$ | dopant atom concentration in a crystalline grain |
| P | hole conduction |
| r | radius of grinding cylinder |
| R | resistance |
| S | resistivity of a crystalline grain divided by the electron charge |
| t | film thickness |
| t | time |
| T | temperature |
| V | voltage |
| $V_f$ | volume of a film |
| $V_{gb}$ | volume of the grain boundary region within a film |
| x | width of grooved area |
| x | length of conducting layer |
| $\gamma$ | multiplying factor |
| $\mu$ | mobility |
| $\mu_e$ | mobility of an electron |
| $\mu_{gb}$ | mobility of a charge carrier in the grain boundary regions |

| | |
|---|---|
| $\mu_h$ | mobility of a hole |
| $\mu_i$ | intrinsic mobility |
| $\mu_s$ | mobility of a charge carrier in a crystalline grain |
| $\rho$ | resistivity |
| $\rho^*$ | apparent resistivity |
| $\sigma$ | conductivity |
| $\Omega$ | resistance, ohms |

Abstract

The electrical resistivity of polycrystalline silicon films has been investigated. The films were grown by the chemical vapor decomposition of silane on oxidized silicon wafers. The resistivity was found to be independent of dopant atom concentration in the lightly doped regions but was a strong function of dopant levels in the more heavily doped regions. A model, based on high dopant atom segregation in the grain boundaries, is proposed to explain the results.

# Chapter I

# INTRODUCTION

The electrical and structural properties of single crystal silicon are well known and have been the subject of extensive reviews (for example, see References 1-7). Single crystal silicon has been largely responsible for the tremendous growth in the electronics industry during the past 20 years as it is the base material for integrated circuits, silicon vidicon cameras, and other photon detectors, charge coupled devices and most transistors and diodes.

Silicon of high purity and crystalline perfection is required for most applications. Recently, however, polycrystalline silicon has become important for application in constructing a new class of field-effect transistors[8,9], charge-coupled devices[10,11,12], field shielded devices[13], and dielectrically isolated integrated circuits.[14,15]

The most important aspect of polycrystalline silicon as it is used in the above mentioned applications is its sheet resistance. The polycrystalline silicon interconnections may be long and narrow, hence, the lines may add up to a significant resistance. This resistance, coupled with the capacitance of the underlying oxide may produce a phase shift in the electrical signal between the

beginning of a line and its end. Such phase shifts limit the frequency of operation of the device or limit the length of usable lines. Hence, there exists the need to characterize the behavior of the resistivity of poly-crystalline silicon as a function of doping level, type of dopant, film thickness, and thermal history.

In this thesis the author hopes to extend the knowledge and understanding of the electrical properties of poly-crystalline silicon as influenced by its doping concentration and microstructure. Previous studies of amorphous and polycrystalline silicon will be reviewed and the data obtained from the various investigators will be compared for consistent trends. The small amount of data on dislocation effects on electrical properties will be reviewed for application to grain boundary effects.

In the chapters subsequent to these reviews, the specific experiments performed by the author will be explained in detail. The data obtained from the experiments will then be presented. In the final chapter, a model, representing the polycrystalline film, will be derived. The unknown variables in the model will be obtained by curve fitting the data. The model is based on the assumption the crystalline grains and the grain boundary regions have different conductivity properties and that the majority of the dopant atoms are trapped in the grain boundary.

# Chapter II

# Literature Review

## A. Amorphous Silicon

The study of amorphous semiconductors has centered primarily around the chalcogenide glasses[16,17] which have possible application as memory devices. Although investigations of amorphous silicon and germanium date back more than a decade[18,19,20] no switching has been reported in these materials. This review will concentrate on the elemental amorphous semiconductor - silicon rather than the chalcogenides since different theory may well apply to elemental amorphous semiconductors[21,22] and since the remainder of this dissertation is only concerned with silicon.

Amorphous silicon has been prepared by vacuum evaporation, sputtering and chemical vapor deposition. The criterion for producing amorphous silicon rather than poly-crystalline silicon is the substrate temperature during deposition or during post-deposition heat treatment.

Collins[18] used a resistance heated boron nitride crucible to evaporate silicon onto fused quartz substrates which were held at various temperatures. X-ray data show an amorphous to polycrystalline transition between 400°C and 600°C. The resistivity of these film dropped from

greater than $10^2 \Omega$ cm in the amorphous state to a value between $0.02 \Omega$ cm and $10 \Omega$ cm in the polycrystalline state. Collins also reported that chemical analysis of the deposited films contain approximately 0.5 percent boron (from the boron nitride crucible). The solid solubility limit of boron in silicon is approximately 1 percent[4], hence, the films were very heavily doped with acceptor atoms but the exact doping level was not controlled.

Hass[20] found that deposition on substrates at a temperature less than $600^{\circ}$C produced amorphous films. However subsequent heat treatment produced an amorphous-crystalline transformation at approximately $700^{\circ}$C. Mountvala[23] also found an amorphous to polycrystalline transformation at a deposition temperature of approximately $700^{\circ}$C. The electrical characteristics of his films varied from greater than $10^3 \Omega$-cm for deposition temperatures less than $650^{\circ}$C to approximately $0.1 \Omega$-cm for deposition temperatures greater than $800^{\circ}$C. However, care must be exercised in interpreting this data since the film thickness was not held constant ($500 A^{\circ} \leq t \leq 7500 A^{\circ}$) and the resistivity of polycrystalline silicon films increase as the thickness approaches one micron or less.†

---

†This data will be discussed in a later section of this paper.

Mountvala used both highly doped (arsenic) η-type silicon ($N_d \approx 2.5 \times 10^{18}$ atoms/cm$^3$) and highly doped (boron) p-type silicon ($N_a \approx 10^{20}$ atoms/cm$^3$) as source materials but he found that all films had a p-type nature. Attempts were made to explain this conductivity change as resulting from contamination from the evaporator bell jar.

Walley[24] used an electron beam to evaporate 30 ohm-cm silicon (impurity type was not given) onto unheated glass substrates. It was found that the film resistivity would increase if the pressure of the vacuum chamber rose above $10^{-5}$ torr or the deposition rate fell below 30A°/sec [0.18μm/min]. The resistivity of the silicon films deposited at rates greater than 30A°/min and at pressures less than $10^{-5}$ torr was approximately 50Ω cm.

Onuma and Sekiya[25] deposited silicon on fused quartz by electron beam evaporation. They found that all film deposited on substrates heated to 600°C and below were amorphous.

Kermagai et al.[26] sputtered heavily doped ($N \approx 10^{20}$ atoms/cm$^3$) n and p type (arsenic and boron) silicon onto heated fused quartz substrates. X-ray diffraction produced only very diffuse rings for substrate deposition temperatures up to 400°C. Subsequent heat treatment above 650°C produced clearly defined diffraction rings. The resistivity of one micron thick samples, deposited from a

boron doped source, was greater than $10^4\Omega$-cm until heat treated to $650^oC$ where the resistivity dropped to $1.0\Omega$-cm. Heat treatment in a reducing atmosphere at $1000^oC$ produced a resistivity of $0.1\Omega$ cm. However, silicon films deposited from an arsenic doped (n-type) source remained in a high resistivity ($> 10^4\Omega$-cm) state regardless of heat treatment.

Brodsky et al.[22] sputtered high resistivity silicon onto single crystal sapphire which was held at or below room temperature. Post deposition anneals, in vacuum, of these 0.3 to 10 μm thick films produced an amphorous to crystalline transformation between 400 and $500^oC$. The resistivity of these films increased with each anneal cycle until the anneal temperature reached approximately $300^oC$. The resistivity rose from approximately $4 \times 10^3$ $\Omega$-cm for the as deposited film to greater than $10^6\Omega$-cm.

Le Comber et al[27] measured the electrical properties of amorphous silicon films. Their films were deposited from silane gas in a r.f. heated, glow discharge, reactor. The only variable in the depositions was substrate temperature which was varied from $310^oK$ to $670^oK$. The resistivity data exhibited a tendency to decrease (from $2 \times 10^{11}$ $\Omega$-cm to $10^7$ $\Omega$-cm) as the deposition temperature increased.

Chittick et al.[28] deposited amorphous silicon films on glass substrates by the pyrolytic decomposition of silane. Uniform samples were produced with thickness, of different samples, varying from 0.2 to 4.0 μm. The resistivity of the undoped films dropped from approximately $10^{10}$ ohm-cm for room temperature depositions to approximately $5 \times 10^4$ ohm-cm for $500^\circ C$ depositions. Room temperature depositions in which phosphine ($PH_3$) is added to the silane, show a resistivity dependence as shown in Table I.

TABLE I

Resistivity-vs-Doping Level in Amorphous Silicon (ref. 28)

| $PH_3/SiH_4$ (%) | ρ(ohm-cm) |
|---|---|
| 0.004 | $10^{10}$ |
| 0.01 | $4 \times 10^9$ |
| 0.02 | $2 \times 10^9$ |
| 0.4 | $10^4 - 10^6$ |
| 4.0 | $10^4 - 10^6$ |

Summary

As has been shown, the existing data on amorphous silicon is widely scattered. The results obtained in this review are summarized in Table II.

The significance of the scatter in the data is especially obvious when compared to Irwin's[29] data on the

resistivity of single crystal silicon. In his review he compared the data of thirteen different investigations on the dependence of doping concentration on resistivity and obtained a smooth curve through the data points of which 75 percent of the data points deviate less than 10 percent from the curve.

B. Polycrystalline Silicon films have been deposited by vacuum evaporation and chemical vapor deposition on heated substrates and by the annealing of amorphous films deposited on cold substrates. (The subject of amorphous silicon films and amorphous-polycrystalline transformations were reviewed in the previous section.) Even though limited success has been obtained in growing large grain silicon films on amorphous substrates by first depositing a thin layer of gold[30,31,32], it can be generally assumed that a heated amorphous substrate will nucleate a polycrystalline film. When silicon is deposited on a heated single crystal substrate, of proper lattice spacing, an epitaxial layer may result if the temperature is sufficiently high and the substrate sufficiently clean.

In this section, the author will first discuss previous findings on the crystalline preferred orientations and grain sizes. The existing data on electrical properties will then be discussed. It will be found that the older

Table II. - Reported Properties on Amorphous Silicon

| Reference | Deposition Method | Dopant & Level | Resistivity (ohm-cm) before anneal-after anneal | Temperature of Amorphous-Poly-crystalline Trans-formation |
|---|---|---|---|---|
| Collins,[18] | Resistance Heated evaporation | Boron, .5% | $>10^2$ - 0.02 | 400-600°C |
| Hass,[20] | | | | 600-800°C |
| Mountvala, 23 | Electron beam evaporation | Boron, $10^{20}/cm^3$ | $>10^3$ - 0.1 | 700°C |
| | | Arsenic $2.5x10^{19}$ | $>10^3$ - 0.1 (p type) | 700°C |
| Walley,24 | Electron beam evaporation | -, $\approx 3 \times 10^{14}$ | 50 | - |
| Kumagai, 26 | Sputter | Boron, $10^{20}$<br>Arsenic, $10^{20}$ | $>10^4$ Ωcm-~1.0 to 0.1<br>$>10^4$ ->$10^4$ | 650°C<br>650°C |
| Broadaky, 22 | Sputter | Intrinsic, | $4x10^3$ - $>10^6$ (at 300°C) | 400-500°C |
| Chittick, 28 | CVD, silane | Boron, $3x10^{14}$<br>Phor, 0.004%-4% | $10^{10}$ - $5x10^4$<br>$10^4$ to $10^{10}$ | |

data will be quite scattered but that the more recent data will have much less scatter and be in reasonable agreement with the data obtained here.

1. Structure

Collins[18] found an increasingly strong (111) preferred orientation of vacuum deposited polycrystalline silicon on fused quartz as the substrate temperature was increased from 600°C to 1100°C. He reported that the films became progressively coarser and less continuous as temperature was raised. Kataoka[33] also found a (111) preferred orientation for 3.5 μm thick films which were evaporated from tantalum filaments onto hot (temperature range, 950-1050°C) fused quartz.

King et al[34] obtained only random orientation in polycrystalline films evaporated on thermally oxidized silicon wafers when the substrate temperature was between 600 and 730°C. Films deposited on substrates heated above 730°C had a (111) preferred orientation. All films were approximately 2500°A thick.

Heaps et al.[35] deposited silicon by chemical vapor deposition from trichlorosilane ($SiHCl_3$) in hydrogen. They obtained a polycrystalline film with no preferred orientation. The substrate was a single crystal of silicon heated to 900°C. No grain size information was given.

Mountvala and Abowitz[23] grew polycrystalline silicon on fused quartz substrates heated from 765°C to 1000°C. They used an electron beam evaporation system. The preferred orientation in the (110) orientation increased as temperature increased to 900°C where the (111) orientation became competitive.

"Submicron" polycrystalline silicon grains were obtained[36] by the chemical vapor deposition of silicon from silicon tetrachloride ($SiCl_4$) on oxidized silicon substrates heated to 1150°C. The films were deposited at 2μm/minute for 10 minutes.

Sirtl and Seiter[37] used a mixture of $CH_3SiHCl_2$, $SiHCl_3$, and $H_2$ to produce polycrystalline silicon films on single crystal silicon substrates. Transmission electron photomicrographs showed a grain size near the limit of resolution for a 1050°C deposition temperature. High deposition temperatures produced larger grains.

A crystalline structure[9] consisting of closely packed platelets with dimensions on the order of 100A° was found in silicon films approximately 1000A° thick. These films were deposited on oxidized silicon by the thermal decomposition of silane at temperatures ranging from 650°C to 750°C. No preferred orientation data was given.

Previous investigations conducted by the author[38,39] have shown a preferred orientation in thick silicon layers

deposited by the thermal decomposition of silane on oxidized silicon. The preferred orientation was both thickness and temperature dependent. A maximum in the (110) preferred orientation occurred at the deposition temperature of 1000°C. The diameter of the grains at the surface of 16 μm thick sample was approximately 1 μm throughout the temperature range (840°C to 1170°C).

Kamins et al.[40,41,42] report that the grain size of 20 μm thick silicon films deposited under similar conditions as the author's films were 2 to 3 μm across at the surface but were "many times smaller" when the film thickness was on the order of 1 μm. Their work on preferred orientation agreed with references 38, 39 except at deposition temperatures below 900°C where a local increase in the (110) preferred orientation is shown.

Cowher and Sedgwick[43] found that the grain size of 2 μm thick silicon films deposited on oxidized silicon by the silane process was doping level dependent. The reported data was obtained on films grown at 650°C with deposition rate of 600A°/min. (0.06 μm/min). These data are summarized in Table III below.

Table III

Silicon Microstructure-vs-Doping Level (ref. 43)

| Doping Concentration Boron, atoms/$cm^3$ | Grain Size A° | Grain Orientation |
|---|---|---|
| $10^{14}$ | 250 - 350 | Random |
| $10^{17}$ | 900 - 1100 | Mostly Random |
| $10^{19}$ | 2000 - 3000 | (110) |

2. Electrical Properties

In six of the papers to be reviewed here, the deposition conditions have already been described in the section on Polycrystalline Silicon: Structure, and here the information will not be repeated. A comparison of structural properties, deposition parameters, and electrical properties will be made in a table at the end of this chapter.

Collins[18] found that once past the crystallization temperature, the resistivity of heavily doped (boron) silicon films increased as a function of deposition temperature. The resistivity went from approximately 0.02 ohm-cm for deposition temperatures of 600-700°C to approximately 10Ω-cm at 800-1000°C.

Kataoka[33] grew polycrystalline silicon films by evaporation on heated fused quartz substrates from tantalum filaments. He started with n-type single crystals with a doping level of approximately $7 \times 10^{14}$ atoms/$cm^3$. Films deposited on 950oC and 1000°C substrates had p-type carriers, but a very high resistivity ($\approx 10^5 \Omega$-cm). A 10 minute anneal at the deposition temperature reversed the conductivity type of the 1000°C deposition and a 40 minute anneal lowered the resistivity by about three orders of magnitude. Heat treatment, at the deposition temperature, for as long as 30 minutes did not change the conductivity type of the 950°C deposition. Kataoka also found that the Hall mobility increased from 50 to 120 $cm^2$/volt sec as the deposition, with anneal, temperature increased. It is not clear if the mobility increase is due to structural changes or to the change in the type of carrier.[†]

Mountvala and Aborwitz[23] found that the resistivity of polycrystalline silicon dropped from about 2.5Ω-cm when deposited at 755°C to about 0.1Ω-cm for deposition temperatures of 835°C - 1000°C. They used both n and p-type starting materials but they reported that

---

[†]In single crystal silicon, at room temperature, the mobility of electrons is approximately three times greater than the mobility of holes[44].

all of their films were p-type.

Sirtl and Seiter[37] tried doping their polycrystalline silicon films during the deposition step but could not obtain reproducible results. For a given deposition both the carrier concentration and the mobility were increased by a 1200°C anneal in oxygen. Typical results are given in Table IV below. The films were 150μ thick and were doped during deposition with phosphorous from phosphine ($PH_3$) in molar ratios of $PH_3$:Si compounds = $10^{-5}$.

Table IV

Electrical Properties of Polycrystalline Silicon (ref. 37)

| Film Condition | Carrier Concentration (carriers/$cm^3$) | Resistivity (Ω-cm) | Mobility ($cm^2$/V·sec) |
|---|---|---|---|
| As grown | $4.5 \times 10^{15}$ | 60 | 23 |
| 4 hr anneal | $2.1 \times 10^{16}$ | 8.6 | 34 |
| 8 hr anneal | $7.4 \times 10^{16}$ | 5.8 | 15 |

Bean et al.[45] grew a polycrystalline silicon rod from undoped trichlorosilane ($SiHCl_3$) or silicon tetrachloride ($SiCl_4$) at a temperature greater than 1100°C. Although the grain size was not given, it was reported that the grains grew as needle like crystallites similar to those grown by Fripp[38] and Kamins[46] from silane ($SiH_4$). Electrical measurements were made on samples cut both parallel and

perpendicular to the direction of growth of the needles. The same group of investigators also measured the electrical properties of thick (10-16 mil) films of polycrystalline silicon deposited from various sources on different substrates[47]. The results of both papers are shown in Table V below.

Table V

Electrical Properties of Polycrystalline Silicon (ref. 45 and 47)

| Sample | Resistivity (Ω-cm) | Mobility ($cm^2/V\cdot cm$) | Carrier Concentration ($cm^{-3}$) |
|---|---|---|---|
| Cut parallel to grain growth | $5.2 \times 10^4$ | 430 | $2.8 \times 10^{11}$ |
| Cut perpendicular to grain growth | $3.2 \times 10^5$ | 33 | $5.8 \times 10^{11}$ |
| Cut perpendicular to grain growth | $5.9 \times 10^5$ | 49 | $2.1 \times 10^{11}$ |
| $SiH_4$ on $Si_3N_4$ at 930°C | $1.5 \times 10^3$ | <1 | $>10^{15}$ |
| $SiH_4$ on $SiO_2$ at 930°C | $8.9 \times 10^3$ | <1 | $>10^{14}$ |
| $SiHCl_3$ on $SiO_2$ at 1100°C | $6.5 \times 10^4$ | <1 | $>10^{14}$ |
| $SiCl_4$ on $SiO_2$ at 1150°C | $1.5 \times 10^5$ | <1 | $>10^{13}$ |
| $SiCl_4$ on $Si_3N_4$ at 1200°C | $1.4 \times 10^5$ | 5.0 | $9 \times 10^{12}$ η-type |
| $SiCl_4$ on SiC at 1200°C | $1.3 \times 10^5$ | 7.7 | $6.3 \times 10^{12}$ η-type |

| Sample | Resistivity (Ω-cm) | Mobility ($cm^2/V \cdot cm$) | Carrier Concentration ($cm^{-3}$) |
|---|---|---|---|
| $SiCl_4$ on $SiO_2$ at 1200°C | $1.4 \times 10^5$ | 1.4 | $3.3 \times 10^{13}$ η-type |
| $SiCl_4$ on Si† at 1200°C | $3.1 \times 10^1$ | 1780 | $1.1 \times 10^{14}$ η-type |

†Epitaxial film, substrate was highly doped ($N \approx 10^{18}$ atoms/$cm^3$) η-type single crystal.

No reason was given for the large differences in mobility and carrier concentration when measured on the dielectric substrates and when measured on cut samples. Commercial grade silane and silicon tetrachloride normally have background dopant concentrations of approximately $10^{13}$, per cubic centimeter[48]; hence in the latter set of data there appears to be a source of contamination and in the former set there appears to be a loss of carriers. The range of resistivity values appear to be consistent for both sets of their data but is significantly higher than that measured by Fa and Jew[36] when they obtained 50Ω-cm films grown from silicon tetrachloride ($SiCl_4$) at 1150°C.

T. I. Kamins[49] and Joseph and Kamins[40] of the Fairchild Research and Development Laboratory have performed research on a polycrystalline silicon system which is similar to that reported in this dissertation. In these investigations, polycrystalline silicon was deposited from

silane ($SiH_4$) onto thermally oxidized silicon. The silane was diluted with hydrogen and mixed with either arsine ($AsH_3$) or diborane ($B_2H_6$) to provide (when desired) dopant atoms. An induction heated horizontal epitaxial reactor was used for depositions.

The resistivity of undoped polycrystalline silicon was measured[40] and found to be nearly independent of film thickness (0.5μm - 2.5μm) deposition temperature (650 ± 1040°C) and growth rate (0.12 to 0.5 μm/min). The resistivity of all films was between $10^5$ - $10^6$Ω-cm, and the temperature effects on resistivity indicate an activation energy of 0.4 - 0.6 ev.

The Hall mobility and carrier concentration were measured on moderately to heavily doped ($N > 10^{17}$ atoms/cm$^3$) polycrystalline silicon[49]. These films were deposited at 1035°C and were about 5 μm thick. The data obtained from this investigation are shown in Table VI below. In the table Na or Nd is the density of dopant atoms (boron or arsenic) alloyed into the film during deposition whereas $n_e$ or $n_h$ is the density of charge carriers in the film as determined from the Hall data.

Table VI

Electrical Properties of Polycrystalline (ref. 49)

| Na atoms/cm$^3$ | $n_h$ carriers/cm$^3$ | $\mu_h$ cm$^2$/V·sec | ρ ohm-cm |
|---|---|---|---|
| $1.1 \times 10^{17}$ | $1.8 \times 10^{16}$ | 8 | 43 |
| $2.1 \times 10^{17}$ | $3.9 \times 10^{16}$ | 18 | 8.9 |
| $10^{18}$ | $2 \times 10^{17}$ | 30 | 1.04 |
| $4.5 \times 10^{18}$ | $2 \times 10^{18}$ | 48 | .065 |
| $9 \times 10^{18}$ | $5 \times 10^{18}$ | 44 | .028 |
| $3.\ 10^{19}$ | $3 \times 10^{19}$ | 35 | 0.006 |

| $N_d$ | $n_e$ | $\mu_e$ | ρ |
|---|---|---|---|
| $1.2 \times 10^{17}$ | $2 \times 10^{17}$ | 5 | 6.25 |
| $4 \times 10^{17}$ | $1.8 \times 10^{17}$ | 20 | 1.7 |
| $1.3 \times 10^{18}$ | $8 \times 10^{17}$ | 25 | 0.34 |
| $1.5 \times 10^{18}$ | $1.2 \times 10^{18}$ | 34 | 0.15 |
| $2.5 \times 10^{18}$ | $2 \times 10^{18}$ | 20 | 0.15 |
| $4 \times 10^{18}$ | $3.5 \times 10^{18}$ | 32 | 0.056 |

†The resistivity was not given in the paper but was calculated from the carrier concentration and Hall mobility data.

Cowher and Sedgwick[43] measured the resistivity of undoped polycrystalline silicon and the Hall mobility and carrier concentration of heavily doped films. All films were 2 μm thick and were grown at 650°C from silane-hydrogen ($SiH_4$-$H_2$) mixtures in an induction heated reactor. The doping gases used were phosphine and diborane ($PH_3$ and $B_2H_6$).

The measurement of donor concentration was not repeatable, even though the ratio of $PH_3$ to $SiH_4$ was controlled, until the alloy level of phosphorus in the silicon film exceeded $10^{19}$ atoms/cm$^3$. Qualitatively boron films exhibited a similar relationship but an exact dopant level was not known. The data from this paper is summarized in Table VII below.

Table VII

Electrical Properties of Polycrystalline Silicon (ref. 43)

| $\frac{B_2H_6}{SiH_4}$ | $N_a$ atoms/cm$^3$ | $n_h$ carriers/cm$^3$ | $\mu_h$ cm$^2$/V·sec | $\rho$ ohm-cm |
|---|---|---|---|---|
| $10^{-4}$ | - | $\sim 10^{14}$ | ~200 | 312 |
| $10^{-4}$ | - | $\sim 5 \times 10^{16}$ | ~100 | 1.25 |
| $10^{-4}$ | - | $\sim 7 \times 10^{16}$ | ~ 3 | 30 |
| $10^{-4}$ | - | $\sim 10^{17}$ | ~ 1 | 62 |
| $10^{-4}$ | - | $\sim 10^{-8}$ | ~ 7 | 0.9 |
| $10^{-4}$ | - | $5 \times 10^{18}$ | ~ 10 | 0.125 |
| $10^{-4}$ | - | $10^{19}$ | ~ 10 | 0.06 |
| $7 \times 10^{-4}$ | - | $7 \times 10^{19}$ | ~ 10 | 0.009 |
|  | Undoped | - | - | $\sim 10^{6}$ |

Table VII (cont'd.)

| $\frac{PH_3}{SiH_4}$ | $N_d$ | $n$ | $\mu_h$ ($cm^2$/V·sec) | $\rho$ |
|---|---|---|---|---|
| $3x10^{-5}$ | $10^{19}$ | $5 \times 10^{14}$ | 1000 | 12.5 |
| $2x10^{-5}$ | $10^{19}$ | $2 \times 10^{16}$ | 1000 | 0.31 |
| $2x10^{-5}$ | $10^{19}$ | $2 \times 10^{17}$ | 800 | 0.04 |
| $2x10^{-5}$ | $10^{19}$ | $5 \times 10^{18}$ | 8 | 0.16 |
| $6x10^{-5}$ | $2x10^{19}$ | $10^{19}$ | 9 | 0.07 |
| $10^{-4}$ | $4x10^{19}$ | $2 \times 10^{19}$ | 8 | 0.04 |
| $8x10^{-3}$ | - | $8 \times 10^{19}$ | 8 | 0.01 |

The resistivity of undoped and of very heavily doped polycrystalline silicon was also measured by Eversteyn and Put[50]. Their films were grown from silane in an induction heated reactor and their substrates were oxide coated silicon wafers. The resistivity of undoped films was greater than 500Ω cm and the resistivity of the heavily doped films was dependent on the deposition temperature since the concentration of doping gas going into the reactor was sufficiently high to exceed the solid solubility limits in the crystal. There was a large drop in resistivity (5 - 0.005Ω cm) for deposition temperatures greater than 620°C. The resistivity continued to drop slowly to the maximum deposition temperature (1000°C).

Table VIII

Reported Properties of Polycrystalline Silicon

| Reference | Deposition Method | Dopant and Level (atoms/$cm^3$) | Resistivity (ohm-cm) | Preferred Orientation | Substrate Type |
|---|---|---|---|---|---|
| 18 | Vacuum evaporation | Boron, ~$10^{20}$ | .02 to 10 | (111) | Fused quartz |
| 33 | Vacuum evaporation | n-type,~ | $10^2$ to $10^5$ | (111) | Fused quartz |
| 34 | Vacuum evaporation | | | (111) | Oxidized silicon |
| 35 | Chemical vapor deposition | | | None | Single crystal silicon |
| 23 | Vacuum evaporation | Arsenic and boron | 0.1 to 2.5 | (110) | Fused quartz |
| 50 | Chemical vapor deposition | Boron,~$10^{20}$<br>Phosphorus ~$10^{20}$ | ~.005<br>~.005 | | |
| 37 | Chemical vapor deposition | See table IV | | | |
| 40,41,42 | Chemical vapor deposition | See table VI | | (110) | Oxidized silicon |
| 43 | Chemical vapor deposition | Boron, $10^{14}$<br>Boron,$10^{19}$ | See Table VII | Random<br>(110) | Oxidized silicon |

C. Dislocations

Shockley[51] introduced the concept that the row of unpaired atoms of an edge dislocation would have dangling unpaired electrons which would act as acceptor sites. These acceptor sites are along the dislocation lines and, in a n-type material, they would become negatively charged until the repulsive electrostatic energy would balance the decrease in energy of an electron dropping from the conduction band edge into the dislocation, acceptor, site.

Read[52,53] extended the theoretical model to include the possibility of the existing unpaired electron of the dislocation half plane becoming a donor in p-type material. It was hypothesized that a single dangling electron would be easier to ionize than an electron that was in a normal tetrahedral bond.

Glaenger and Jorden[54,55] used Read's theoretical work as a guide to perform electrical measurements on dislocations in silicon. They measured the lifetime of excess carriers and the resistivity of both n-type and p-type silicon which had approximately $10^7$ dislocations/$cm^2$. The data indicated the existence of an acceptor site 0.52 ev below the conduction band and a donor site between 0.38 and 0.5 ev above the valence band. However, the source of the trapping sites is not necessarily due to dislocations, as the papers hypothesized, since lifetime measurements before

deformation were not reported and the data reported could easily be attributed to a low concentration of gold in the silicon.

D. Grain Boundaries

As is well known (for example, see ref. 56), low angle grain boundaries may be described by dislocation networks. Although Read's theory[52] did not include systems in which the space charge regions would overlap, such as is possible in grain boundaries, the concept of dislocations at a grain boundary introducing acceptor and donor sites is still quite valid.

Electrical properties of grain boundaries in germanium have been investigated by many laboratories[57-61] but the only previous work found on grain boundaries in silicon was that of Matukura[62,63]. Matukura made his samples by growing bands of silicon from two seed crystals which were rotated with respect to each other. Apparently though, his grain boundaries were wide enough to have electrical connections made to them without the possibility of shorting to the single crystal regions. This grain boundary would have to be at least 25 μm wide, hence this author believes that the data is not to be trusted.

# Chapter III

## Experimental Procedures

The polycrystalline silicon films were grown on oxidized single crystal silicon by the pyrolytic decomposition of silane. Oxidized silicon is amorphous, hence, the silicon films produced were polycrystalline.

The experimental procedures used in this paper ranged from substrate preparation to film characterizations. The basic steps of the experiments were:

1. Oxidation of the single crystal silicon wafers.
2. Pyrolytic decomposition of silane for silicon film deposition.
3. Resistivity measurements.
4. Transmission electron microscopy and optical microscopy.
5. Post deposition heat treatment.

Each of these steps will be discussed separately.

(1) Oxidation of the Single Crystal Silicon Wafers

The silicon wafers used in these experiments were 1 ohm-cm single crystals sliced parallel to the (111) plane and were purchased with a lapped and polished surface. After being cleaned according to the steps in table IX, the wafers were oxidized, by the procedure in table X. Figure 1 shows the oxidation apparatus. The oxide produced

in this manner was between 5000 and 6000 $A^{o}$ in thickness. The lack of color variation in the thin oxide indicates that the surface was flat and smooth.

Table IX - Cleaning Procedure for Silicon Wafers

| Solvent | Time |
|---|---|
| Trichloroethylene, Ultrasonic bath | 10 minutes |
| Boiling Trichloroethylene | 30 minutes |
| Methanol | Rinse |
| D.I. Water | Rinse |
| Nitric Acid ($80^{o}C$) | 20 minutes |
| D. I. Water | Three Rinses |
| Methanol | Storage |
| $N_2$ (gas) | Blow off methanol before oxidation. |

Table X

Oxidation Procedure

| | |
|---|---|
| Furnace Temperature | $1100^{o}C$ |
| Furnace Tube | Fused Quartz |
| Water Temperature | $94^{o}C$ |
| Carrier Gas (for $H_2O$ vapor) | $N_2$ |
| Gas Flow Rate | 1 ℓ/min |
| Time | 50 min. |

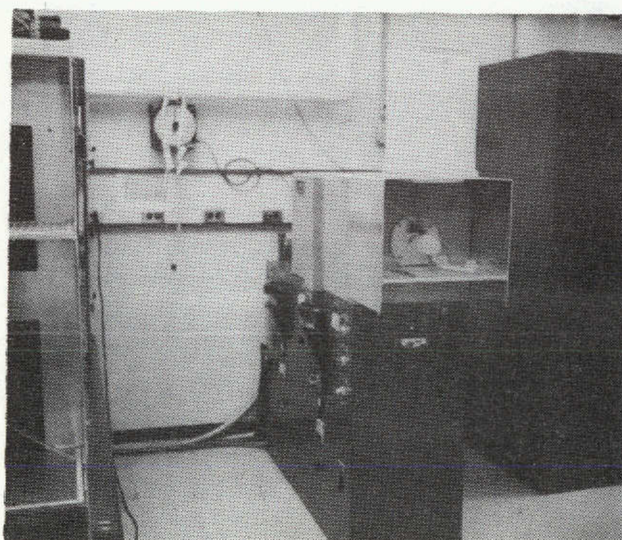

This page is reproduced at the back of the report by a different reproduction method to provide better detail.

Figure 1.- Silicon oxidation system.

(2) Pyrolytic Decomposition of Silane for Silicon Film Deposition

Silane ($SiH_4$) gas is one of the standard sources used by many electronic companies for the epitaxial growth of silicon. Commonly used sources of phosphorus and boron for doping the silicon during growth is phosphine ($PH_3$) gas and diborane ($B_2H_6$) gas. The beginning and final chemical states are given in equations 1-3.

$SiH_4(g)$ ----- $Si(s) + 2H_2(g)$ (1)

$2PH_3(g)$ ----- $2P(s) + 3H_2(g)$ (2)

$B_2H_6$ -------- $2B(s) + 3H_2(g)$ (3)

The system (figure 2) that was used for the silicon deposition was a standard induction heated horizontal epitaxial reactor. Water cooled copper pipe is used as a primary winding to heat a silicon coated graphite susceptor located on a quartz rack inside a 30 x 2 1/2 inch fused quartz tube.

Hydrogen is used as a carrier gas and it is purified by passing it through a liquid nitrogen cold trap. Hydrogen is first in the gas lines and it mixes with the other gases as they are fed through their flow meters into the line going to the reaction chamber. The flow rate of hydrogen is much higher than the flow rate of silane which, in turn, is much higher than the flow rates of the doping gases. The flow rates typically used are given in Table XI below.

Table XI

Flow Rates of Gases Used in Depositing Silicon

| Gas | Purpose | Flow Rate |
|---|---|---|
| $H_2$ | Dilution - Carrier | 13,600 ml/min |
| $SiH_4$ | Silicon Source | 50 ml/min |
| $PH_3$ or $B_2H_6$ | Dopant Source | 0 to 0.03 ml/min |

The purpose of the high hydrogen flow rate is to sufficiently dilute the silane and dopant gas to retard gas phase reaction and to insure a sufficient velocity of reactants to obtain a uniform deposition rate over the area of the susceptor which holds the substrates. The flow rate of the dopant gas was adjusted to obtain the desired doping level of impurity atoms in the silicon crystal.

The susceptor was made in house since a suitable susceptor could not be purchased. Four depressions were milled into a flat, rectangular graphite block to provide convenient, reproducible placement of the silicon wafers and to prevent them from slipping off of the susceptor. The graphite block was then cleaned in a manner similar to that of the silicon wafers before oxidation. After being cleaned and dried, the graphite block was placed in the reactor and approximately 3 μm of silicon was deposited on it at 1070°C. The temperature was then raised above

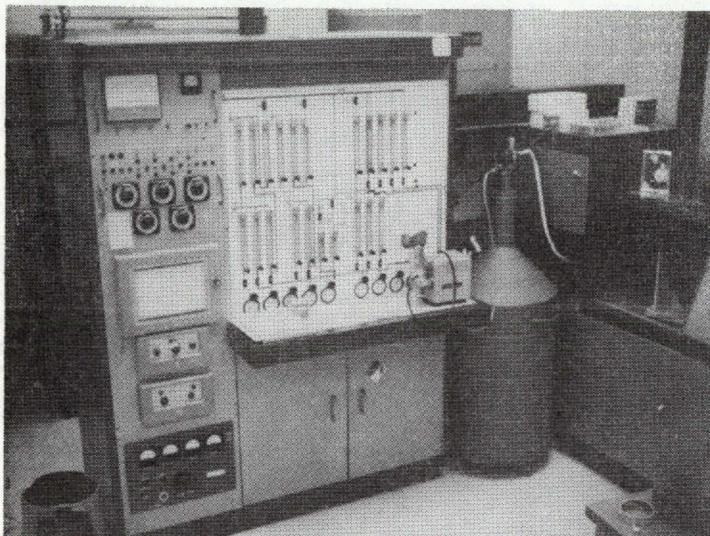

a.- Control Panel

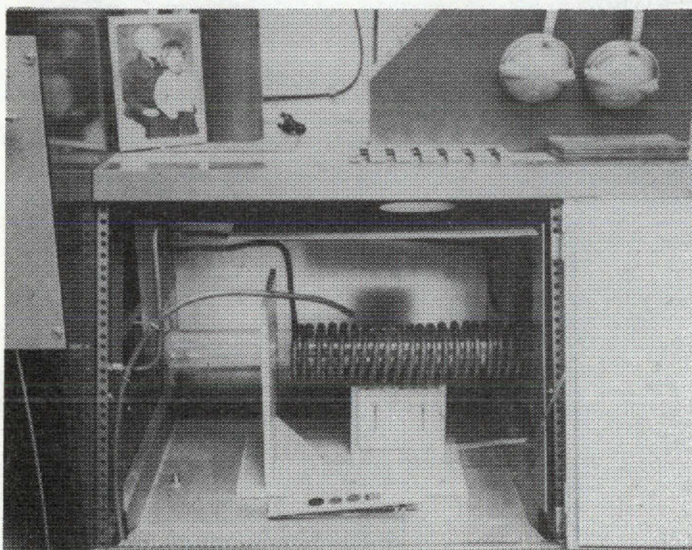

b.- Reaction Chamber

Figure 2.- Silicon deposition system.

This page is reproduced at the back of the report by a different reproduction method to provide better detail.

the melting point of silicon and much of the silicon appeared to be absorbed by the graphite. The temperature was then lowered back down to 1070°C and another 5 μm silicon was deposited. Two susceptors were constructed in order to have a separate one for each of the doping gases. The susceptors were periodically etched in the reactor with anhydrous HCl at 1200°C to prevent excessive silicon build up.

The temperature of the susceptor was set by a calibrated optical pyrometer and controlled by a recording optical pyrometer. The optical pyrometer was calibrated by constructing a graphite black body adjacent to a silicon wafer on the susceptor and plotting a curve of the apparent temperature of the silicon verses the graphite temperature. The accuracy of this method was checked by sighting the pyrometer on a silicon wafer in a tube furnace of known temperature. At 1100°C the two temperature measurements differed by 5°C.

The reactor was continuously purged with nitrogen during non operating times. After the susceptor, with substrates on it, was placed in the reactor tube the nitrogen flow was turned off and the system was flushed with hydrogen. Power was then applied to the induction coil and the susceptor was brought up to 1170°C in less than one minute. Four minutes after first applying power, the

temperature was reduced to 1070°C for one set of depositions and left at 1170°C for another set of depositions, that is, two different deposition temperatures were investigated. The system was allowed to stabilize at the deposition temperature for two minutes and then the reacting gases were introduced into the system. The deposition time varied from 5 seconds to 10 minutes. After the deposition ended the system was allowed to flush with hydrogen, at temperature, for one minute. The power was then turned off and the wafers were cooled in flowing hydrogen.

In each run, four substrates were placed on the susceptor. Two of the substrates were oxide covered and would grow polycrystalline films. The other two substrates were single crystals and would produce epitaxial layers. The epitaxial films functioned as monitors for system cleanliness and they also provided a method of determining the doping atom concentration in the polycrystalline films. This method of determining the dopant atom concentration is not exact. If four single crystals are used for substrates, both the epitaxial layer thickness and resistivity will vary from wafer to wafer. However these variances are small (±25%) when compared to the range of doping concentration used in the experiments. The thickness variation between polycrystalline films and epitaxial films was approximately the same as between epitaxial films in similar positions.

(3) Resistivity Measurements

The film resistivity was obtained from Smits' equation (reference 64);

$$\rho = 4.5 \frac{V}{I} t \tag{4}$$

where

$\rho$ = resistivity in ohm-cm

V = voltage, in volts, between the inner two probes of a four point probe

I = current, in amperes, through the outer two probes of a four point probe

t = film thickness in centimeters

The four-point probe system is shown in figure 3. The measurements taken on this system were compared with those taken on a commercially available system for low resistivity samples. However, the input impedance of the voltmeter on the commercial unit prevented its use to make measurements on high resistivity samples.

The thickness measurements on films 1 μm thick and thicker were made by grinding a cylindrical groove through the film and into the substrate. The grinding cylinder diameter was 2.54 cm and the films were all less than 10 μm thick, hence, equation 5, obtained from the geometry shown in figure 4, can be closely approximated by equation 6.

$$t = \left[r^2 - \left(\frac{x_1}{2}\right)^2\right]^{1/2} - \left[r^2 - \left(\frac{x_2}{2}\right)^2\right]^{1/2} \quad (5)$$

$$t = \frac{x_2^2 - x_1^2}{8r} \quad (6)$$

where

$x_1$ and $x_1$, and $r$ are defined in figure 4.

Thickness measurements of films less than one micron were obtained by selectively etching the polycrystalline silicon to produce a cross grid on the surface and then taking a thickness profile with a Sloan Dektac. The cross grid was produced by photolithography. The hardened photo resist was used as the final mask and the silicon was etched with an acid mixture† that would dissolve silicon twenty-five times faster than silicon dioxide.

(4) Transmission Electron Microscopy and Optical Microscopy

The polycrystalline silicon films were examined by transmission electron microscopy and diffraction and by optical microscopy. The purpose of these examinations was to determine the grain size of the films.

The transmission electron microscope used in these experiments was a Hitachi HU-11B. The silicon samples

---

† †The acid mixture was 2 parts hydrofluoric, 15 parts nitric, and 5 parts acetic.

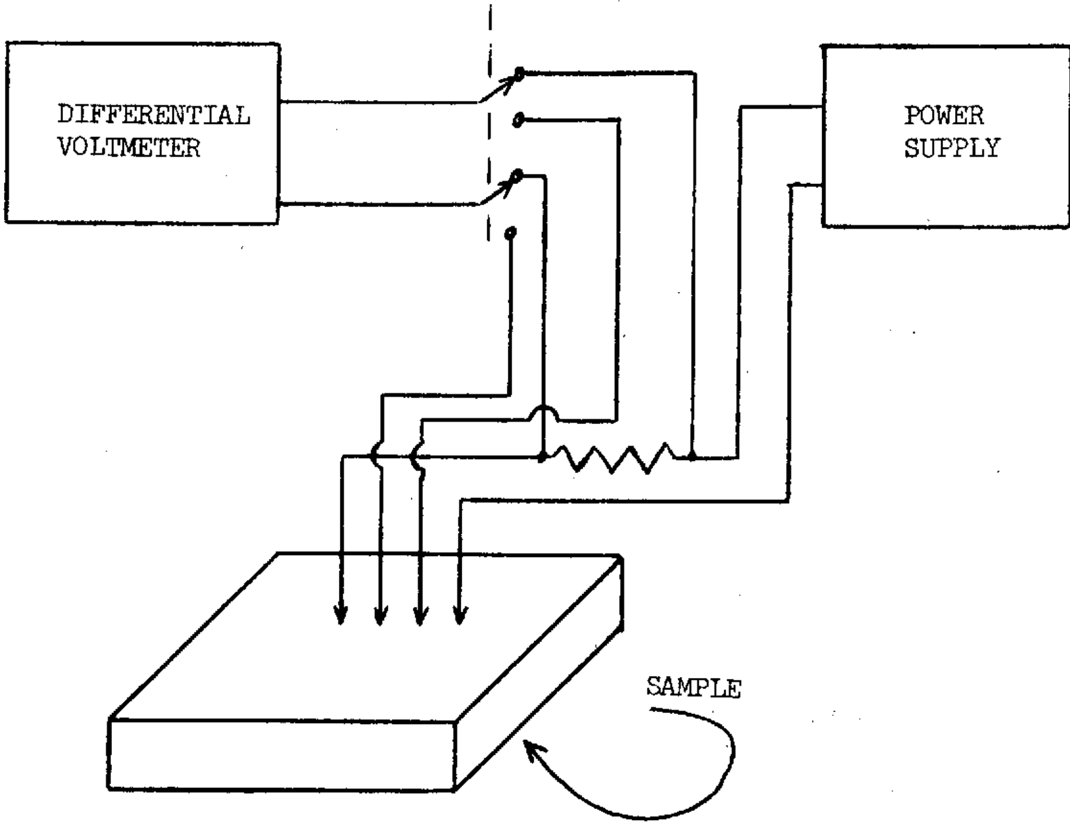


FIGURE 3. — FOUR POINT PROBE SYSTEM

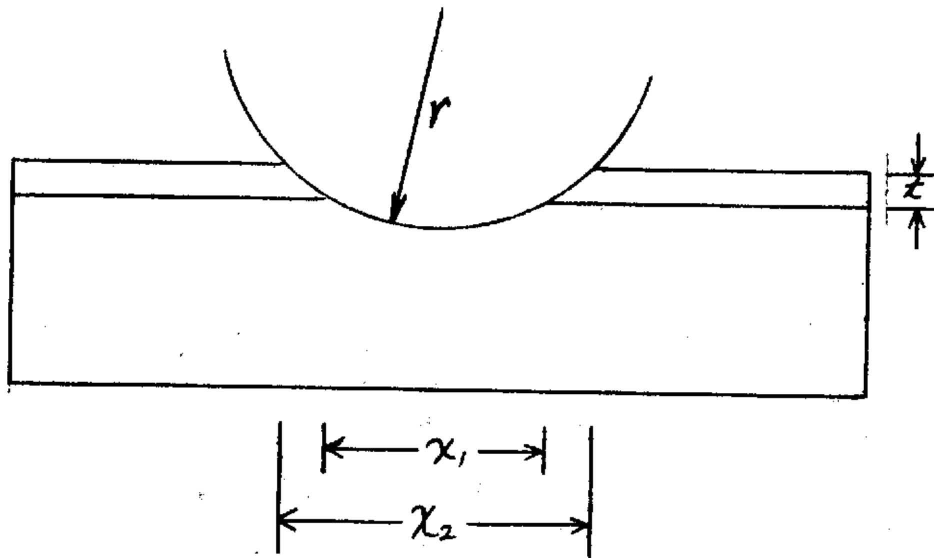


FIGURE 4. — MEASUREMENT OF FILM THICKNESS

were prepared by chemically etching away the substrate and then sputter etching the polycrystalline film to thin it. The chemical etching was performed by waxing the wafer, polycrystalline silicon side down, to a teflon disk. The center of the wafer was left exposed. The teflon disk was rotated in a cylindrical beaker on a magnetic stirrer, by placing one edge of the disk on the plastic coated magnet which was in the beaker. This rotating, stirring, action produced a uniform etch. The silicon wafer was first etched away with the preferential silicon etch that was described previously and then the film of silicon dioxide was removed with dilute hydrofloric acid. Small pieces of the polycrystalline film were placed on copper grids and sputter etched to obtain samples thin enough to be used in the microscope.

A Zeiss Ultrapht Metallograph was used for optical examination of the polycrystalline silicon films. The films were first examined in the as grown condition to check the quality and uniformity of growth.

One objective of the optical examination was to measure the grain size as a function of film thickness. To perform this experiment, the sample was lapped down at a $1^{o}$ angle from the top surface through the oxide and into the single crystal silicon. This lapping step produced a flat surface that exposed the grains at all thicknesses

of the film. The different grains were distinguished by the following oxidation process.

Deal[65] has shown that the silicon oxidation rate is orientation dependent at 1000°C and less. The (111) and (110) faces oxidize at the same rate while the (100) orientation oxidizes at a slower rate. The silicon oxide films are transparent and exhibit thickness dependent characteristic colors due to light interference. Hence different grain orientations can be distinguished by color difference. Single crystal wafers of (100) and (111) orientations were oxidized simultaneously with the polycrystalline sample. The (100) orientated wafers had a yellow-green color under fluorescent lights and the (111) wafers were purple. The polycrystalline samples were multicolored since the different crystallographic orientations oxidized at different rates.

(5) Post Deposition Heat Treatments

A number of samples representing the entire doping range were chosen for post deposition heat treatments. The experiments were performed in the same oxidation furnace as shown in Section I of this Chapter and the conditions, except time, were also the same as in the oxidation step. After a heat treatment which lasted from fifteen minutes to 43 hours, the wafers were removed from the furnace and cooled in air. A film of oxide formed on the surface during

the heat treatment and it had to be removed, by chemical etch, before resistivity measurements could be performed.

# Chapter IV

## Experimental Results

The results obtained through performance of the experiments described in the last chapter will be presented in different sections. The resistivity vs doping level measurements will be described first since these measurements are the main subject of the thesis, and the remainder of the measurements were performed to explain these results.

### A. Resistivity vs. Doping Level

In the first part of this section on resistivity vs. doping levels, only data taken on films grown under "standard conditions" will be discussed. These "standard conditions" are given in table XII. Departure in growth conditions from those of table XII were made to test for resistivity dependence, and these results will be described later.

Table XII

Standard Growth Conditions

| | |
|---|---|
| Temperature | $1070^{o}C$ |
| Deposition Time | 10 minutes |
| Hydrogen Flow Rate | 13,600 ml/min |

Table XII.- (Continued)

| | |
|---|---|
| Silane Flow Rate | 50 ml/min |
| Post Deposition Heat Treatment | None |
| Dopant | n-type; phosphorous |

The phosphorous doping level was varied from 6 x $10^{14}$ atoms/$cm^3$ to 1.5 x $10^{18}$ atoms/$cm^3$. All of the films in this group had similar surface texture and grain size. The thickness of the polycrystalline films was approximately 5.5 μm. The data obtained on these films is given in Table XIII and plotted in Figure 5. The large scatter in the nearly intrinsic resistivity measurements of low doping levels, with the steep descent in resistivity and with additional doping levels for concentrations greater than $10^{16}$ atoms/$cm^3$ is not predictable from previous data on single crystalline silicon (for example see Ref. 29).

In order to establish an end point of the resistivity at the lowest doping levels, two runs were made with no doping gas in the reactor. A clean reactor tube and susceptor were used to insure low levels of unintentional doping. The actual dopant levels were too low to be measured in the single crystal monitors, since the epitaxial films were doped only from the substrates (ie, a p-type substrate produced a p-type epitaxial film and a

n-type substrate produced a n-type epitaxial film); hence, it will be assumed that the doping level is on the order of $10^{13}$ atoms/cm$^3$, n-type, as specified by the silane manufacturer[48]. The resistivity of these polycrystalline films was of the same order of magnitude as all phosphorus doped films with intentional doping levels less than $10^{16}$ atoms/cm$^3$.

Another set of data points was taken to test the dependence of resistivity on dopant type. The boron producing gas, diborane, was used to produce p-type films; all other growth parameters were the same as in Table XII. The data obtained for this set of films are given in Table XIV and plotted in Figure 6. Although the doping level range for boron was not as broad as the phosphorus doped films the similar shape of the curves is obvious. The surface texture and grain size of the boron doped films was the same as the phosphorus doped films.

### B. Resistivity vs Deposition Temperature

A data set was made in which all deposition parameters except temperature were exactly the same as in Table XII. In this set of films the deposition temperature was 1170$^{\circ}$C.

The resistivity of the high temperature deposited films is given in Table XV. Figure 7 plots resistivity as a function of dopant level, and again the curve is similar to figure 5.

Table XIII

Resistivity, Film Thickness, and Doping Concentration for Phosphorous Doped Polycrystalline Silicon Films. Deposition Temperature = 1070°C Deposition Time = 10 minutes.

| Run | Doping Level (atoms/cm$^3$) | Film Thickness (microns) | Film Resistivity (ohm-cm) | Run | Doping Level (atoms/cm$^3$) | Film Thickness (microns) | Film Resistivity (ohm-cm) |
|---|---|---|---|---|---|---|---|
| 1-23 | $\sim 10^{13}$ | 5.2 | $4.9 \times 10^4$ | 1-7 | $\sim 10^{16}$ | 8.0 | $6.5 \times 10^4$ |
| 1-24 | $\sim 10^{13}$ | 5.8 | $6.1 \times 10^4$ | 1-6 | $1.2 \times 10^{16}$ | 7.0 | $1.2 \times 10^3$ |
| 1-28 | $6 \times 10^{14}$ | 5.7 | $2.6 \times 10^4$ | 1-20 | $1.4 \times 10^{16}$ | 4.7 | $9.6 \times 10^4$ |
| 1-29 | $7.5 \times 10^{14}$ | 5.7 | $1.4 \times 10^5$ | 1-21 | $1.5 \times 10^{16}$ | 4.8 | $2.8 \times 10^4$ |
| 1-22 | $10^{15}$ | 4.7 | $1.2 \times 10^5$ | 1-14 | $8 \times 10^{16}$ | 5.6 | 30.5 |
| 1-30 | $10^{15}$ | 5.6 | $1.1 \times 10^5$ | 1-34 | $1.4 \times 10^{17}$ | 5.7 | 2.2 |
| 1-18 | $10^{15}$ | 6.4 | $2.4 \times 10^3$ | 1-11 | $1.7 \times 10^{17}$ | 7.0 | 15 |
| 1-31 | $1.6 \times 10^{15}$ | 5.3 | $1.1 \times 10^4$ | 1-10 | $\sim 2 \times 10^{17}$ | 6.9 | 33 |
| 1-25 | $2 \times 10^{15}$ | 5.7 | $2.8 \times 10^4$ | 1-9 | $\sim 2 \times 10^{17}$ | 6.5 | 16 |
| 1-19 | $2 \times 10^{15}$ | 5.6 | $3.8 \times 10^5$ | 1-17 | $\sim 6.5 \times 10^{17}$ | | ~0.6 |
| 1-26 | $2.3 \times 10^{15}$ | 5.3 | $2.9 \times 10^3$ | 1-32 | $8 \times 10^{17}$ | 5.2 | 0.35 |
| 1-27 | $4 \times 10^{15}$ | 5.6 | $6.9 \times 10^3$ | 1-33 | $1.5 \times 10^{18}$ | 5.3 | 0.22 |
| 1-1 | $8 \times 10^{15}$ | 7.5 | $7.1 \times 10^4$ | 1-16 | $10^{18}$ | 5.2 | 0.31 |
| 1-8 | $9.5 \times 10^{15}$ | 8.0 | $1.8 \times 10^4$ | 1-12 | $\sim 10^{18}$ | 7.9 | |
| 1-2 | $\sim 10^{16}$ | 5.7 | $2.2 \times 10^4$ | 1-13 | $1.1 \times 10^{18}$ | 6.6 | 0.31 |
| 1-3 | $\sim 10^{16}$ | 5.9 | $1.9 \times 10^4$ | 1-15 | $\sim 1.5 \times 10^{18}$ | | 0.25 |
| 1-4 | $\sim 10^{16}$ | 8.0 | $7.8 \times 10^4$ | | | | |
| 1-5 | $\sim 10^{16}$ | 7.0 | $1.1 \times 10^5$ | | | | |

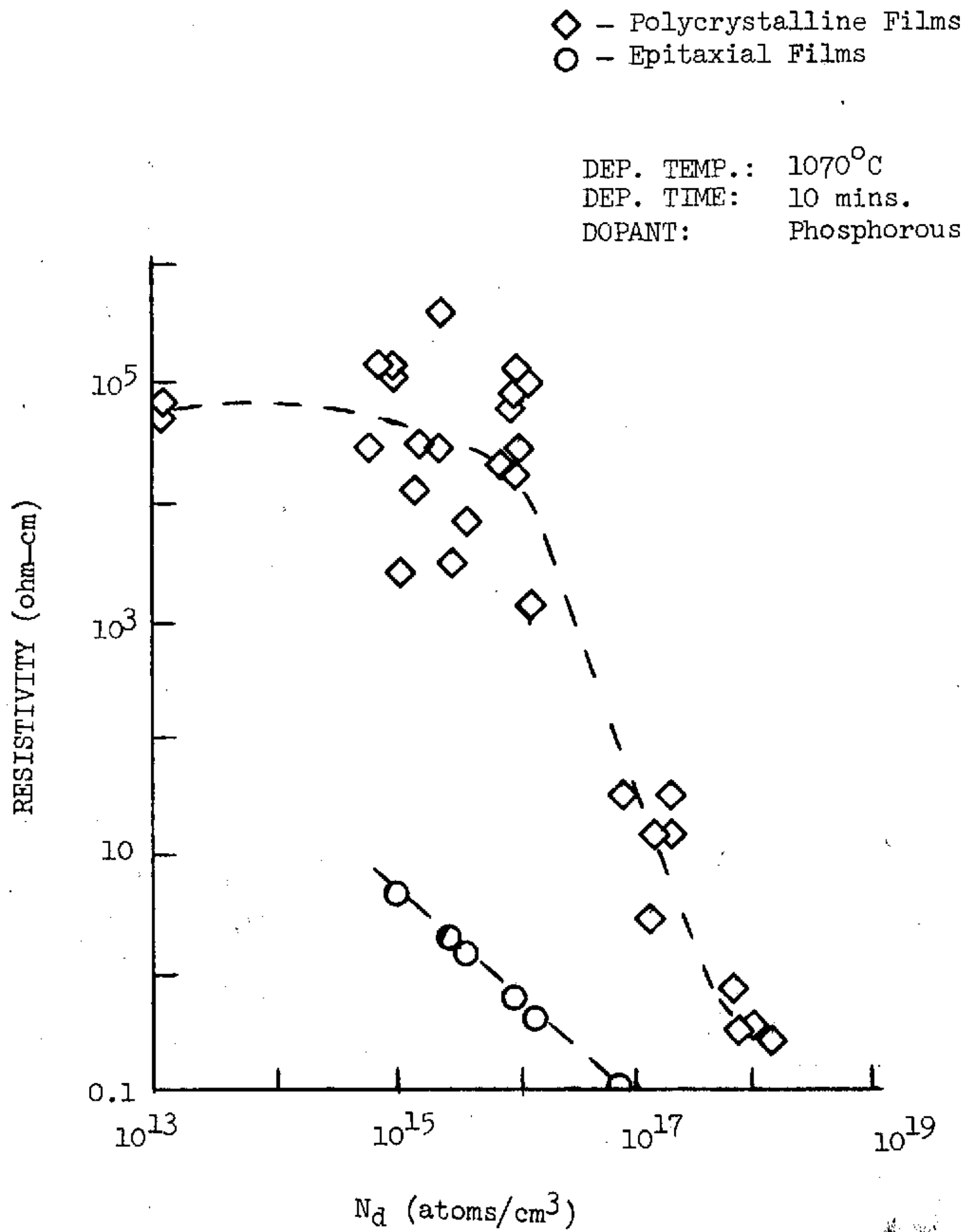


FIGURE 5. – RESISTIVITY OF SILICON FILMS vs. DOPING LEVEL

Table XIV

Resistivity, Film Thickness, and Doping Concentration for Boron Doped Polycrystalline Silicon Films, Deposition Temperature = 1070°C Deposition Time = 10 minutes

| Run | Doping Level (atoms/cm$^3$) | Film Thickness (microns) | Film Resistivity (ohm-cm) |
|---|---|---|---|
| 3-9 | $6 \times 10^{15}$ | 5.9 | $1.1 \times 10^5$ |
| 3-8 | $6.5 \times 10^{15}$ | 5.9 | $7.5 \times 10^4$ |
| 3-7 | $1.5 \times 10^{16}$ | 6.0 | 870 |
| 3-6 | $2 \times 10^{16}$ | 5.9 | $2.5 \times 10^3$ |
| 3-3 | $3 \times 10^{16}$ | 7.1 | $1.5 \times 10^3$ |
| 3-4 | $3.5 \times 10^{16}$ | 5.8 | 350 |
| 3-5 | $3.5 \times 10^{16}$ | 5.4 | 340 |
| 3-1 | $\sim 6 \times 10^{16}$ | 5.7 | 60 |
| 3-2 | $6 \times 10^{16}$ | 5.8 | 42 |

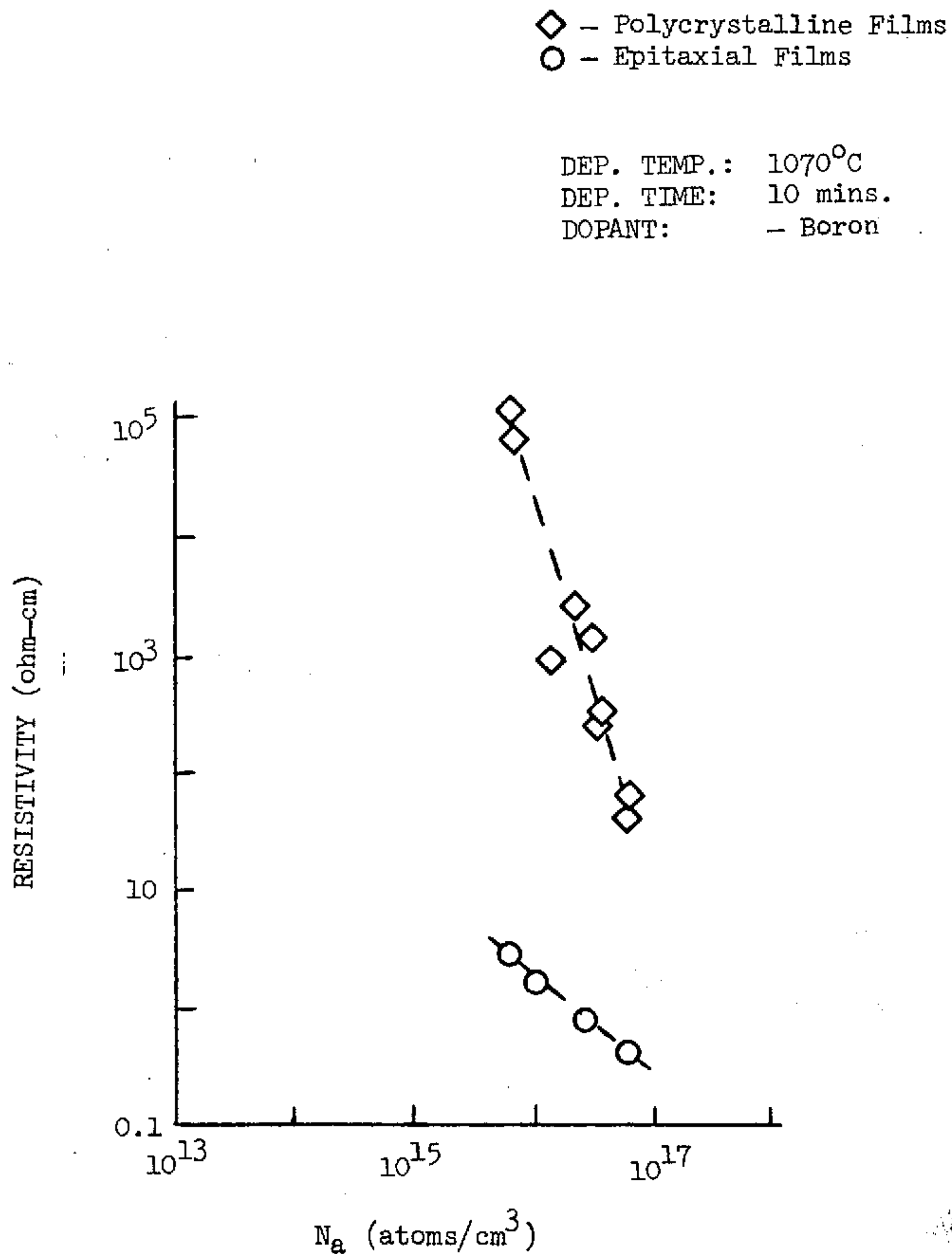


FIGURE 6. – RESISTIVITY OF SILICON FILMS vs. DOPING LEVEL

The grain size was not affected by this difference in deposition temperature, but the higher temperature could have had a strong influence on the redistribution of both host and dopant atoms in the film.

C. Resistivity vs. Film Thickness

A series of films were grown under the standard growth conditions except that the deposition time was varied from 5 seconds to 5 minutes, and two different phosphorous doping levels were used. The data show (see Table XVI and figure 8 and 9) a strong resistivity dependence on thickness for the polycrystalline films and almost no resistivity dependence on the thickness in the single crystal epitaxial layers.

The data obtained on the heavily doped polycrystalline films were more reproducible than those from the lesser doped films, as would be predicted from the data shown in Figure 5.

D. Resistivity vs. Post Deposition Heat Treatment

Based upon the possible existence of a segregation coefficient which would govern the relative concentrations of dopants between the crystalline grains and the grain boundaries, samples from the entire doping range were selected for post deposition heat treatments. It was assumed that a post deposition heat treatment would produce

Table XV

Resistivity, Film Thickness, and Doping Concentration for Phosphorous Doped Polycrystalline Silicon Films, Deposition Temperature = 1170°C Deposition Time = 10 minutes

| Run | Doping Level (atoms/cm$^3$) | Film Thickness (microns) | Film Resistivity (ohm-cm) |
|---|---|---|---|
| 2-3 | $2.6 \times 10^{15}$ | 3.5 | $6.9 \times 10^{3}$ |
| 2-4 | $2.6 \times 10^{15}$ | 3.1 | $1.2 \times 10^{4}$ |
| 2-5 | $2.6 \times 10^{15}$ | 3.3 | $9.1 \times 10^{3}$ |
| 2-6 | $2.6 \times 10^{15}$ | 2.9 | $3.3 \times 10^{3}$ |
| 2-1 | $3 \times 10^{15}$ | 3.7 | $1.1 \times 10^{5}$ |
| 2-2 | $3 \times 10^{15}$ | 3.2 | $4.8 \times 10^{4}$ |
| 2-8 | $2 \times 10^{16}$ | 3.4 | $1.1 \times 10^{3}$ |
| 2-9 | $2 \times 10^{16}$ | 3.3 | $1.1 \times 10^{3}$ |
| 2-10 | $3 \times 10^{16}$ | 2.9 | $1.8 \times 10^{3}$ |
| 2-11 | $10^{18}$ | 2.2 | 0.23 |
| 2-12 | $1.5 \times 10^{18}$ | 3.0 | 0.22 |

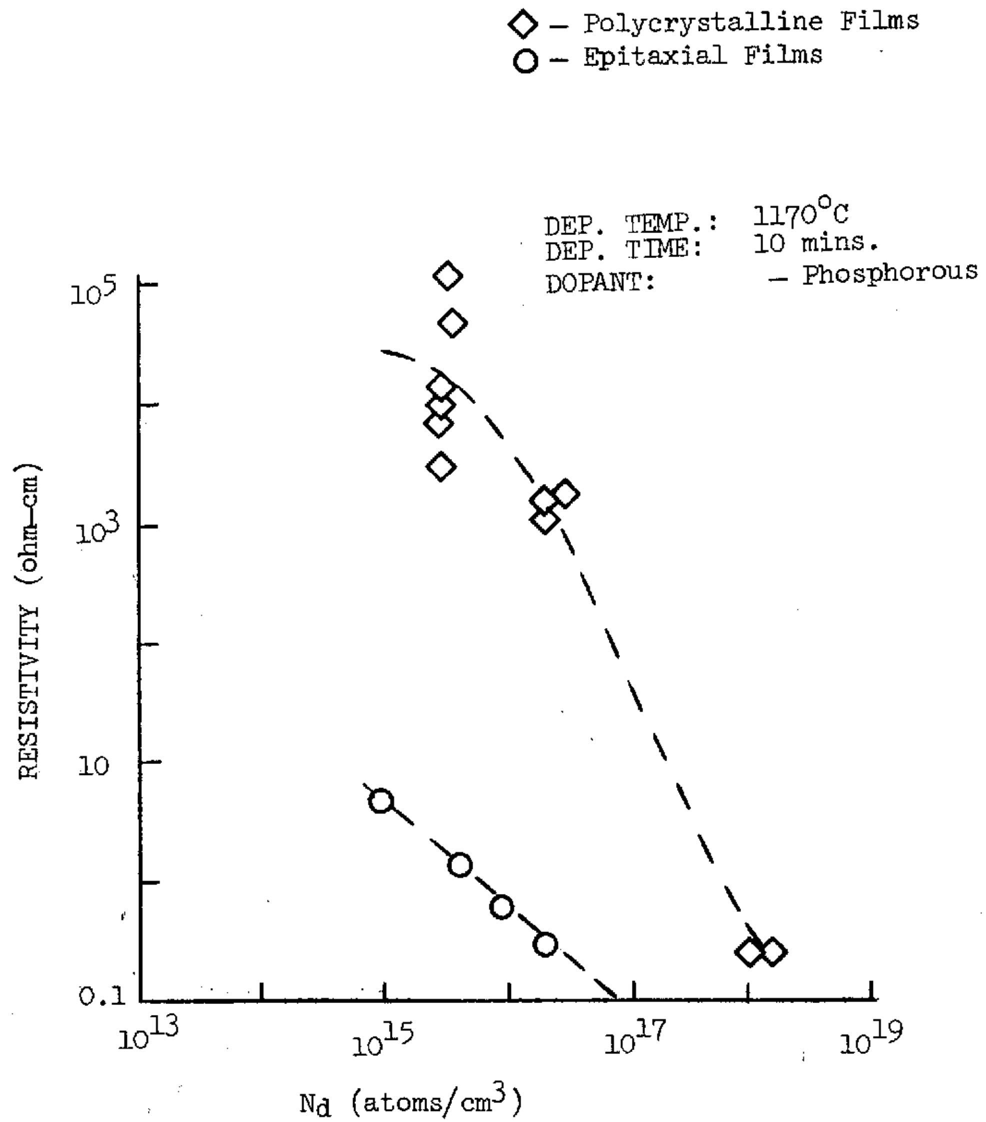


FIGURE 7. – RESISTIVITY OF SILICON FILMS vs. DOPING LEVEL

Table XVI

Resistivity, Doping Concentration, Deposition Time and Film Thickness for Phosphorous Doped Polycrystal and Single Crystal Silicon Films Deposited at 1070°C.

| Run | Doping Level (atoms/cm$^3$) | Deposition Time (sec) | Film Thickness (microns) | Film Resistivity, Polycrystal (ohm-cm) | Film Resistivity, Single Crystal (ohm-cm) |
|---|---|---|---|---|---|
| 4-6P | ~$10^{18}$ | 5 | 0.095 | ∞ | |
| 4-11P | ↓ | 7 | 0.10 | ∞ | |
| 4-5P | | 10 | 0.15 | $1.5 \times 10^3$ | |
| 4-10P | | 15 | 0.17 | 850 | |
| 4-9P | | 20 | 0.21 | 6.8 | |
| 4-4P | | 30 | 0.47 | 6.6 | |
| 4-8P | | 45 | 0.43 | 10 | |
| 4-3P | | 60 | 0.70 | 1.0 | |
| 4-7P | | 90 | 1.0 | 0.28 | |
| 4-2P | | 120 | 1.52 | 0.17 | |
| 4-1P | | 300 | 3.2 | 0.16 | |
| 4-4S | | 30 | 0.41 | | 0.029 |
| 4-8S | | 45 | | | 0.02 |
| 4-3S | | 60 | 0.96 | | 0.03 |
| 4-7S | | 90 | 1.0 | | 0.023 |
| 4-2S | | 120 | 1.66 | | 0.024 |
| 4-1S | ↓ | 300 | 3.4 | | 0.022 |
| 5-3P | ~$2 \times 10^{17}$ | 30 | 0.3 | 273 | |
| 5-9P | ↓ | 30 | 0.3 | 273 | |
| 5-8P | | 60 | | 23.2 | |
| 5-2P | | 60 | 0.6 | 5.2 | |
| 5-5P | | 90 | 0.84 | 34 | |
| 5-7P | | 180 | 0.91 | 2.0 | |
| 5-1P | | 180 | 1.24 | 1.5 | |
| 5-4P | | 300 | 1.8 | 2.5 | |
| 5-3S | | 30 | | | 0.03 |
| 5-3S | | 45 | | | 0.04 |
| 5-8S | | 60 | | | 0.1 |
| 5-2S | | 60 | | | 0.09 |
| 5-5S | ↓ | 90 | 0.65 | | 0.05 |
| 5-7S | | 180 | 1.27 | | 0.05 |
| 5-1S | | 180 | 1.36 | | 0.05 |
| 5-4S | | 300 | 2.1 | | 0.065 |

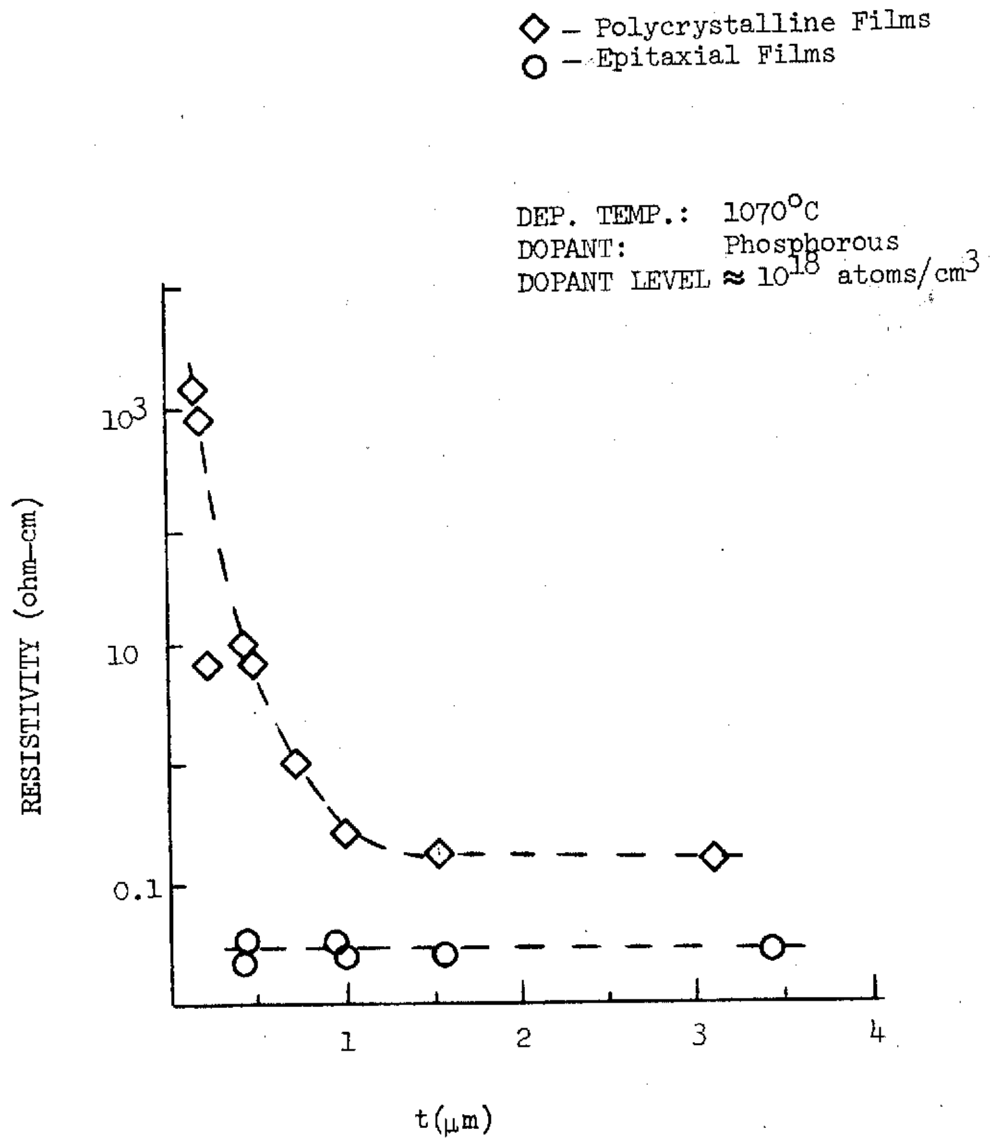


FIGURE 8. – RESISTIVITY OF SILICON FILMS vs. THICKNESS

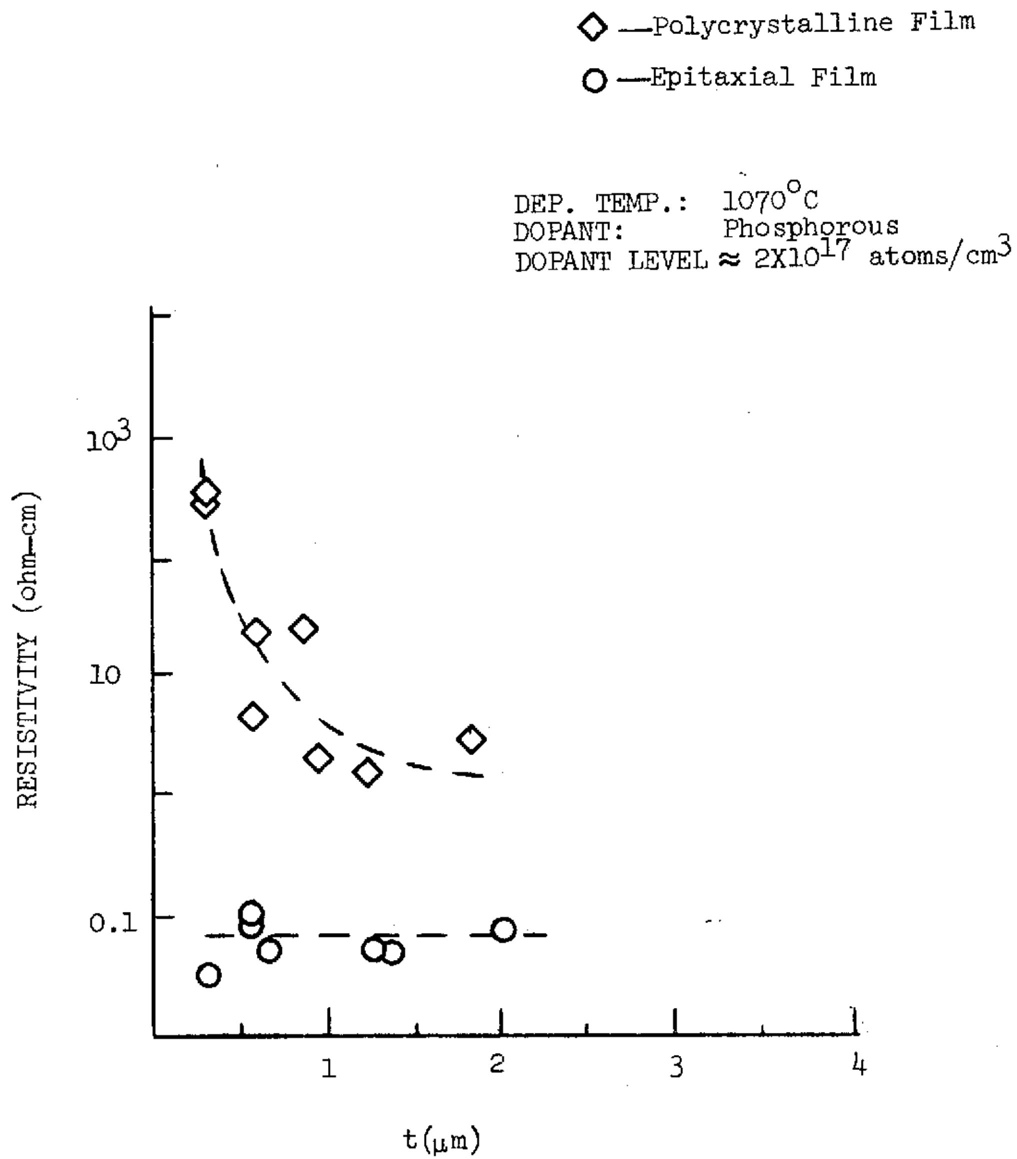


FIGURE 9. – RESISTIVITY OF SILICON FILMS vs. THICKNESS

a more nearly equilibrium distribution of dopants between the interior of the grains and the grain boundaries.

The effects of a post deposition heat treatment in an oxidizing atmosphere were a strong function of the doping level and type. Under no set of conditions was the resistivity significantly decreased but typically the resistivity increased.

The strongest resistivity increases were in the $10^{17}$ atoms/cm$^3$ doping range in phosphorous doped films. Both the high doping end and the low doping end of the curve were only slightly affected by the heat treatment. The original deposition temperature of the films did not affect the final resistivity after heat treatment.

Data taken on oxidized boron doped films were not as extensive as on the phosphorous doped sample. However, the data for the two different doping types show a similar behavior.

The data for a single oxidizing heat treatment is given in Table XVII. Figure 10 is a plot of the post heat treatment resistivity as a function of phosphorous doping level. Once the films were given a single heat treatment in an oxidizing environment, subsequent thermal stress, in a similar environment, had little effect on the resistivity. This is demonstrated by the data in Table XVIII and figures 11 and 12 which compares the

resistivity of the films after one, two, and three oxidation steps. However, in no tests did the resistivity of the epitaxial monitor wafers change measurably.

Neither the oxidation time, nor cooling rate appeared to have a strong influence on the films resistivity. The majority of the samples were given 60-minute heat treatments and a one-minute cooling period, i.e. the silicon boat holding the wafers was withdrawn from the center hot zone of the furnace to an outside cooling rock over a one-minute interval. Other tests were conducted in which the heat treatment time was varied from 15 minutes to 42 hours, and in one test, the boat was withdrawn from the furnace in approximately 2 seconds. Regardless of which procedure was used, the results, as a function of initial resistivity, were nearly the same.

Heat treatments with similar times and temperatures were conducted in a reducing (hydrogen) atmosphere. The results of these tests were consistant within a run but were not reproducible between runs. For example, the resistivity of a set of films might decrease after the first reducing heat treatment, then increase after the second and then decrease again after the third run. The independent variables at work here were not defined and these results will not be considered further.

Table XVII

Resistivity Before and After One Oxidation Cycle, of Doped Polycrystalline Silicon Films, Oxidation Temperature = 1100°C

| Run | Doping Level (atoms/cm$^3$) | Resistivity Before Oxidation (ohm-cm) | Resistivity After Oxidation (ohm-cm) | Oxidation Time (minutes) | Deposition Temperature (°C) | Dopant |
|---|---|---|---|---|---|---|
| 6-19 | $10^{15}$ | $2.2 \times 10^5$ | $2.7 \times 10^5$ | 30 | 1070 | Phosphorous |
| 6-10 | $2 \times 10^{15}$ | $2 \times 10^5$ | $2 \times 10^5$ | 60 | ↓ | ↓ |
| 6-17 | $8 \times 10^{15}$ | 205 | $2 \times 10^5$ | 30 | ↓ | ↓ |
| 6-18 | $8 \times 10^{15}$ | $5.4 \times 10^3$ | $2.6 \times 10^5$ | 30 | ↓ | ↓ |
| 6-9 | $1.5 \times 10^{16}$ | $7.6 \times 10^4$ | $5.3 \times 10^5$ | 55 | ↓ | ↓ |
| 6-3 | $8 \times 10^{16}$ | 30 | $3.3 \times 10^4$ | 60 | ↓ | ↓ |
| 6-15 | $1.2 \times 10^{17}$ | 100 | $1.8 \times 10^4$ | 15 | ↓ | ↓ |
| 6-1 | $1.2 \times 10^{17}$ | 300 | $1.1 \times 10^4$ | 50 | ↓ | ↓ |
| 6-4 | $2 \times 10^{17}$ | 2.6 | 920 | 60 | 1170 | ↓ |
| 6-11 | $4 \times 10^{17}$ | 2.4 | 45 | 60 | 1070 | ↓ |
| 6-6 | $10^{18}$ | 0.27 | 0.71 | 55 | 1170 | ↓ |
| 6-16 | $1.5 \times 10^{18}$ | 0.22 | 0.41 | 30 | 1070 | ↓ |
| 6-2 | $1.1 \times 10^{18}$ | 0.3 | 1.2 | 60 | ↓ | ↓ |
| 6-14 | $5.8 \times 10^{15}$ | $8 \times 10^4$ | $6.5 \times 10^4$ | 60 | ↓ | Boron |
| 6-8 | $6 \times 10^{15}$ | $9.5 \times 10^4$ | $5.7 \times 10^4$ | 55 | ↓ | ↓ |
| 6-13 | $2.3 \times 10^{16}$ | $5.3 \times 10^3$ | $9.8 \times 10^3$ | 60 | ↓ | ↓ |
| 6-5 | $3 \times 10^{16}$ | $1.5 \times 10^3$ | $4.6 \times 10^3$ | 60 | ↓ | ↓ |
| 6-7 | $6 \times 10^{16}$ | 68 | $1.6 \times 10^3$ | 55 | ↓ | ↓ |
| 6-12 | $6.5 \times 10^{16}$ | 65 | $1.1 \times 10^3$ | 60 | ↓ | ↓ |

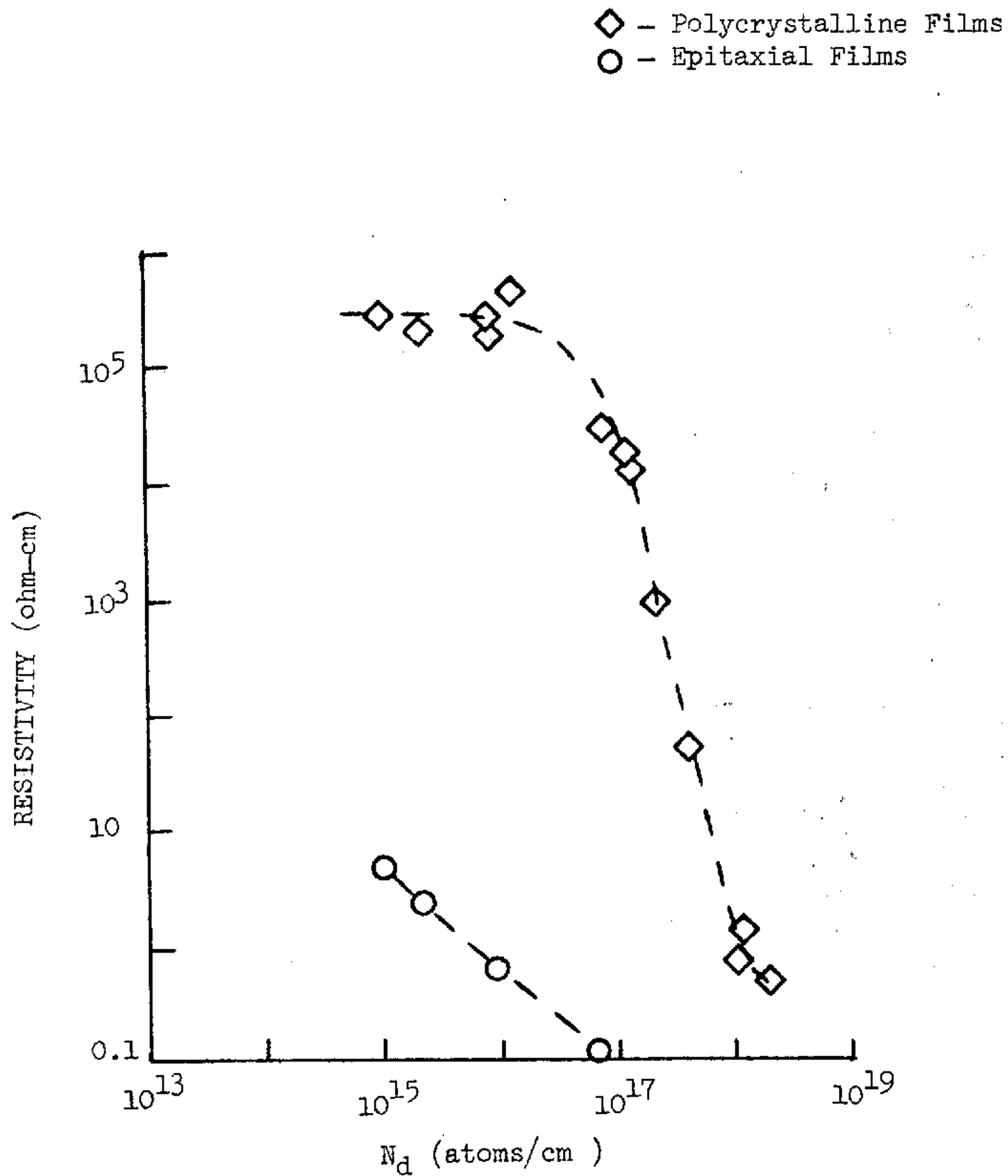


FIGURE 10. – RESISTIVITY OF PHOSPHOROUS DOPED SILICON FILMS AFTER A SINGLE OXIDIZING HEAT TREATMENT AT 1100°C.

Table XVIII

Resistivity Changes in Polycrystalline Silicon Films After Repeated Oxidizing Heat Treatments

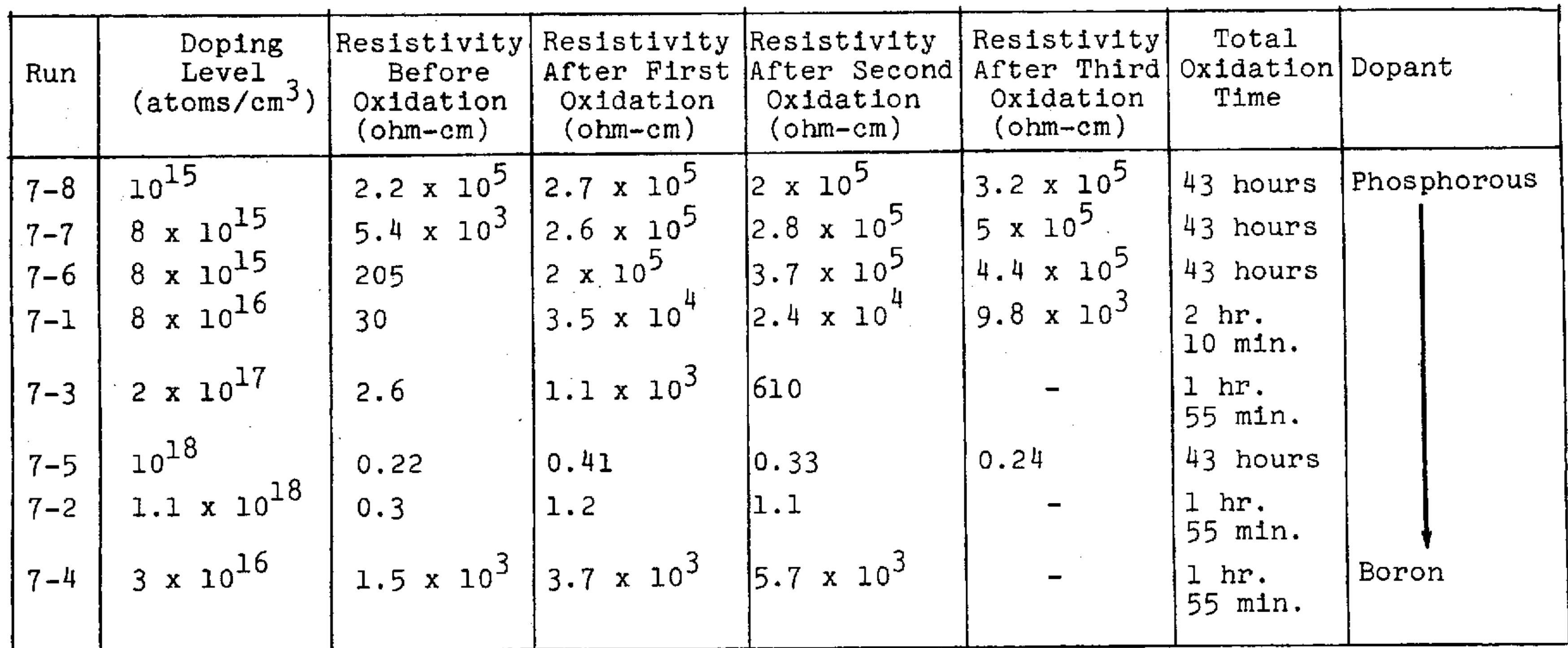

| Run | Doping Level (atoms/cm$^3$) | Resistivity Before Oxidation (ohm-cm) | Resistivity After First Oxidation (ohm-cm) | Resistivity After Second Oxidation (ohm-cm) | Resistivity After Third Oxidation (ohm-cm) | Total Oxidation Time | Dopant |
|---|---|---|---|---|---|---|---|
| 7-8 | $10^{15}$ | $2.2 \times 10^5$ | $2.7 \times 10^5$ | $2 \times 10^5$ | $3.2 \times 10^5$ | 43 hours | Phosphorous |
| 7-7 | $8 \times 10^{15}$ | $5.4 \times 10^3$ | $2.6 \times 10^5$ | $2.8 \times 10^5$ | $5 \times 10^5$ | 43 hours | ↓ |
| 7-6 | $8 \times 10^{15}$ | 205 | $2 \times 10^5$ | $3.7 \times 10^5$ | $4.4 \times 10^5$ | 43 hours | ↓ |
| 7-1 | $8 \times 10^{16}$ | 30 | $3.5 \times 10^4$ | $2.4 \times 10^4$ | $9.8 \times 10^3$ | 2 hr. 10 min. | ↓ |
| 7-3 | $2 \times 10^{17}$ | 2.6 | $1.1 \times 10^3$ | 610 | - | 1 hr. 55 min. | ↓ |
| 7-5 | $10^{18}$ | 0.22 | 0.41 | 0.33 | 0.24 | 43 hours | ↓ |
| 7-2 | $1.1 \times 10^{18}$ | 0.3 | 1.2 | 1.1 | - | 1 hr. 55 min. | ↓ |
| 7-4 | $3 \times 10^{16}$ | $1.5 \times 10^3$ | $3.7 \times 10^3$ | $5.7 \times 10^3$ | - | 1 hr. 55 min. | Boron |

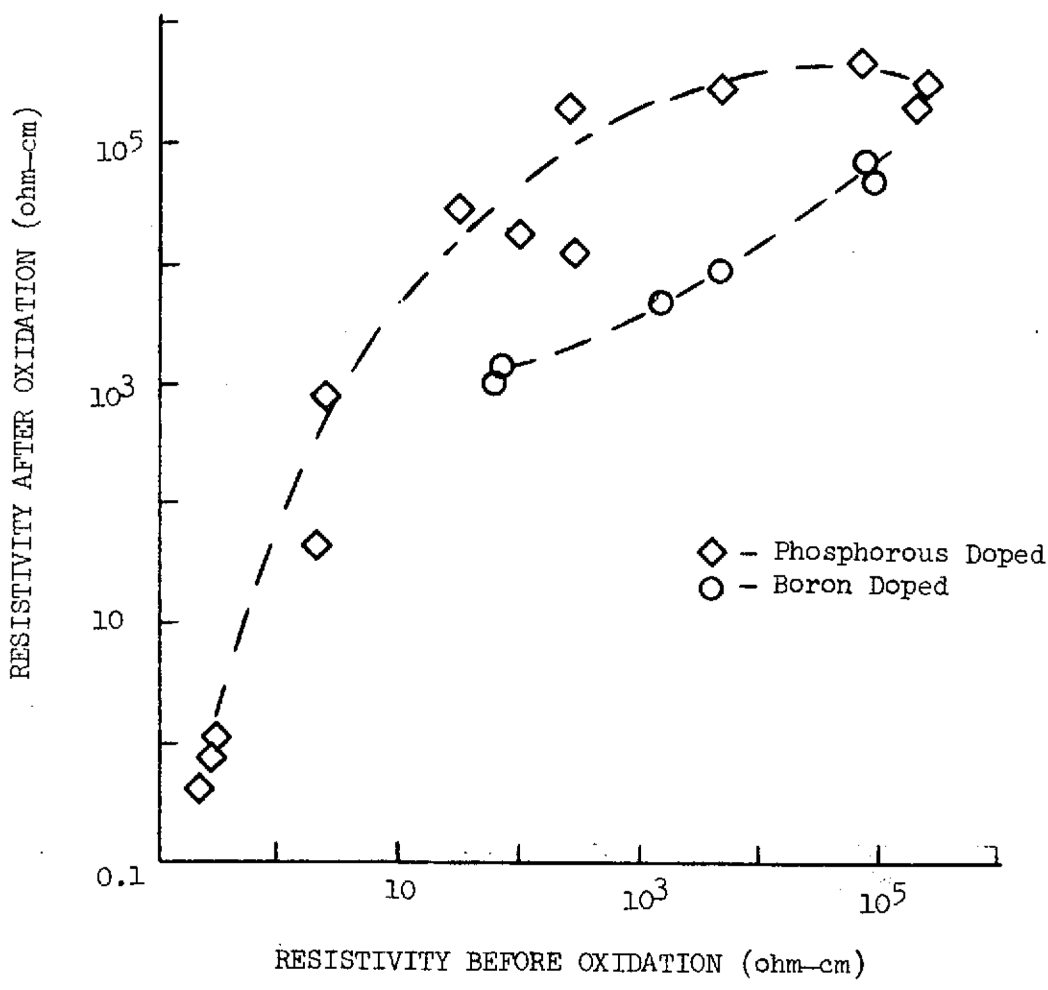


FIGURE 11. – CHANGE IN RESISTIVITY AFTER OXIDATION

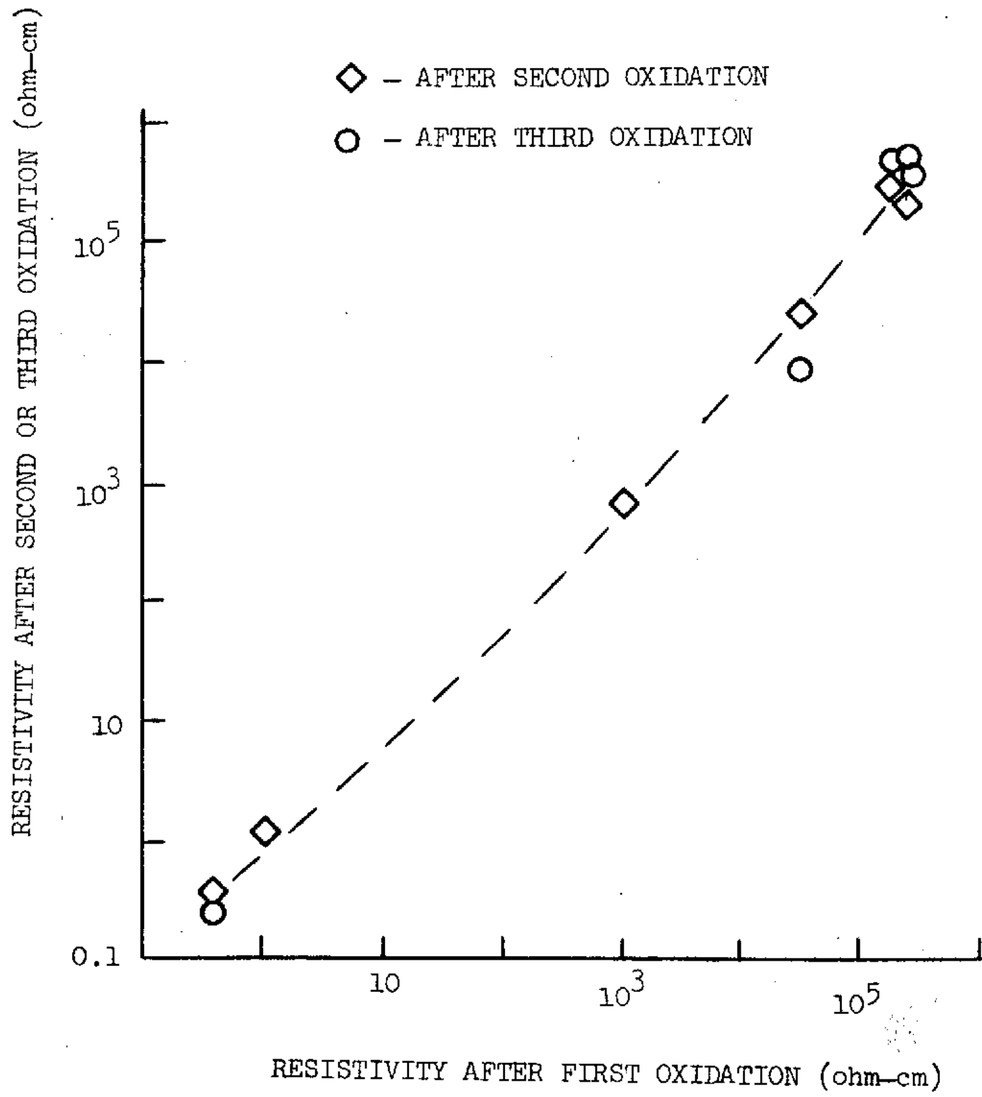


FIGURE 12. – CHANGE IN RESISTIVITY AFTER REPEATED OXIDATIONS

Perhaps the most significant achievement of the heat treatment experiments was to reduce the scatter in resistivity vs doping level in lightly doped polycrystalline silicon. Comparison of the nearness of fit of the data points to the averaged curve in Figures 5 and 10 clearly demonstrates this reduction in scatter.

### E. Grain Size of Crystallites in Films

Examination of thinned polycrystalline films with the transmission electron microscope shows a uniform but fine grained structure (Fig. 13). Electron diffraction photographs (Fig. 14) also show the existence of a fine grained structure with nearly random orientation.

It was desirable to determine the variations of grain size with film thickness in order to determine any correlation between the rise in resistivity with decreasing thickness to a corresponding decrease in grain size. Direct observation with optical microscopy of the film surface was not satisfactory because of the sub-micron grain size of the thinner film but selective oxidation of grains, as explained in the chapter on Experimental Procedures, produced sufficient contrast to obtain a qualitative grain size measurement on films which had been angle lapped. To demonstrate the veracity of the method, a film which had grown some unusually large "spikes" was lapped and oxidized. Before oxidation, no structure was

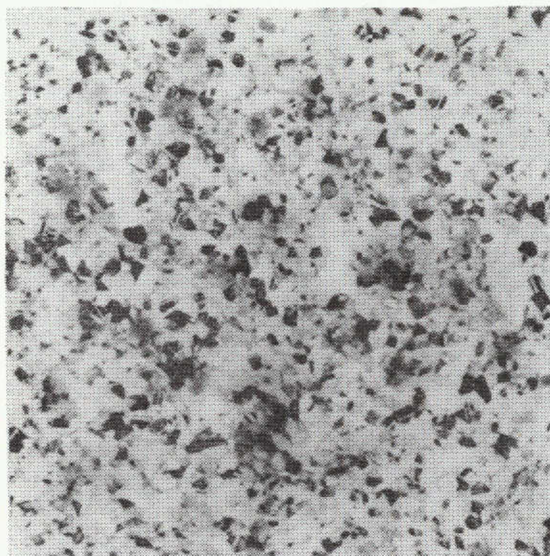

Figure 13.- Transmission electron photomicrograph of silicon film. (21,000X)

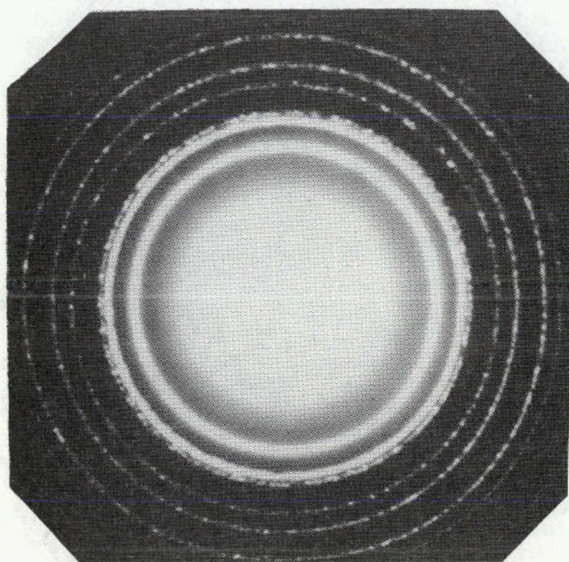

Figure 14.- Transmission electron diffraction patterns.

This page is reproduced at the back of the report by a different reproduction method to provide better detail.

observable but after oxidation the base of the "spikes" were clearly distinguishable and the existence of fine grained structure was visible between spikes (Fig. 15). It was not desirable to take data on this defective film so another film with a smooth uniform surface was lapped and oxidized. Figure 16 shows a series of photographs taken at various positions; hence, the film thickness, on the lapped surface. The pictures are almost identical for thickness above one micron. Below one micron the structure is much finer grained. It would be expected that the film structure would be finer grained at a quarter of a micron than one micron, but what is not expected is for the grain size to terminate at one micron.

Care must be exercised in extrapolating the information given in Figure 16 to very thin films where the films may not be continuous. Continuity occurs at a thickness between 0.1 μm and 0.17 μm as can be seen in Figure 17.

## F. Summary of Results

The resistivity of polycrystalline silicon has been shown to be a widely varying, yet predictable, process dependent property of the material. The resistivity is nearly independent, over the range tested, of deposition temperature and dopant type as can be seen in Figure 18 which combines the data points for all 10 minute depositions. Although the resistivity drops rapidly at the

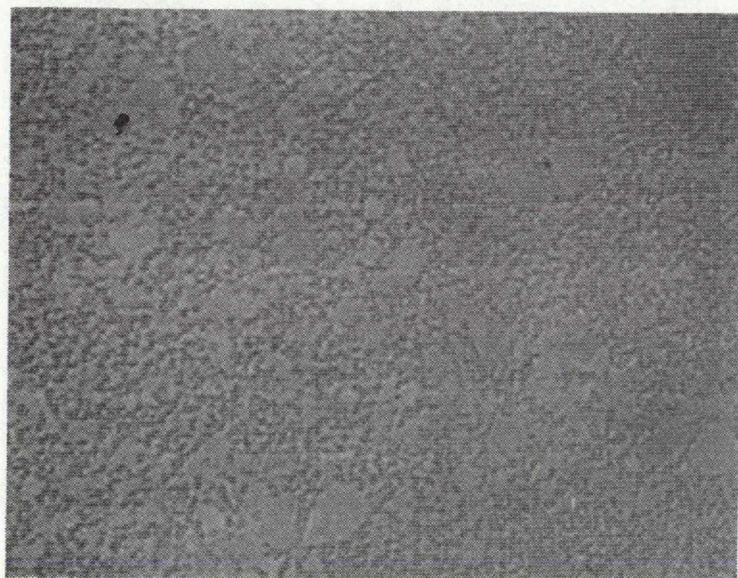

This page is reproduced at the back of the report by a different reproduction method to provide better detail.

Figure 15.- Lapped and oxidized, large grain film. (800X)

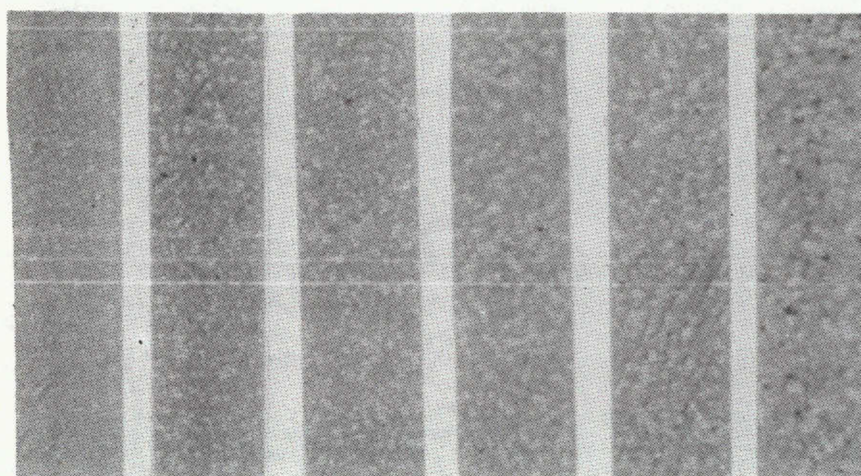

0.25 1.0 2.0 3.0 4.0 5.0

Film Thickness ($\mu$m)

This page is reproduced at the back of the report by a different reproduction method to provide better detail.

Figure 16.- Composite figure showing microstructure vs. film thickness. (800X)

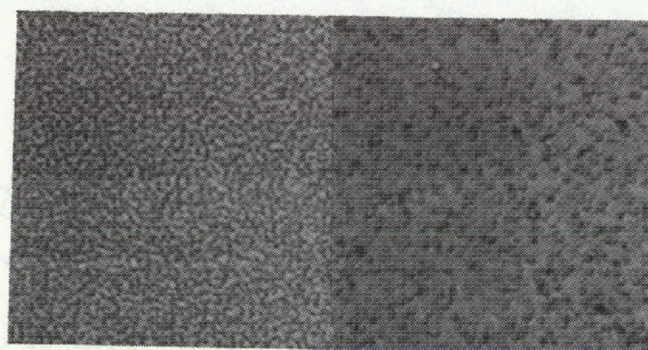

$t \approx 0.10 \mu m$ $t \approx 0.17 \mu m$

This page is reproduced at the back of the report by a different reproduction method to provide better detail.

Figure 17.- Continuous and non continuous films. (1600X)

higher doping levels, it is independent of doping levels in the lower ranges.

The scatter in the data also appears to be related to doping level. The scatter in the resistivity of the deposited films varies over two orders of magnitude in the $10^{15}$ atoms/cm$^3$ doping range and over one order of magnitude at $10^{17}$ atoms/cm$^3$. At high doping levels the scatter is very low.

The wide scatter in the low and intermediate doping ranges is eliminated by a post deposition anneal in an oxidizing atmosphere. Such heat treatment, for as short a time as fifteen minutes; has its strongest effects just below the knee of the curve where the resistivity is raised almost three orders of magnitude. At the low doping end the average resistivity is increased by a factor of four and there is a slight increase at the highly doped end of the curve. The net effect of an oxidizing anneal is to push the knee of the curve out another order of magnitude on the impurity concentration scale, to raise the resistivity of the films with impurity concentration less than $10^{17}$ atoms/cm$^3$ to intrinsic silicon values (see Figure 19) and to eliminate scatter in the data.

It is shown that the anneal step performed in the steam atmosphere was truely oxidizing because a surface film of silicon dioxide was formed. The kinetics of

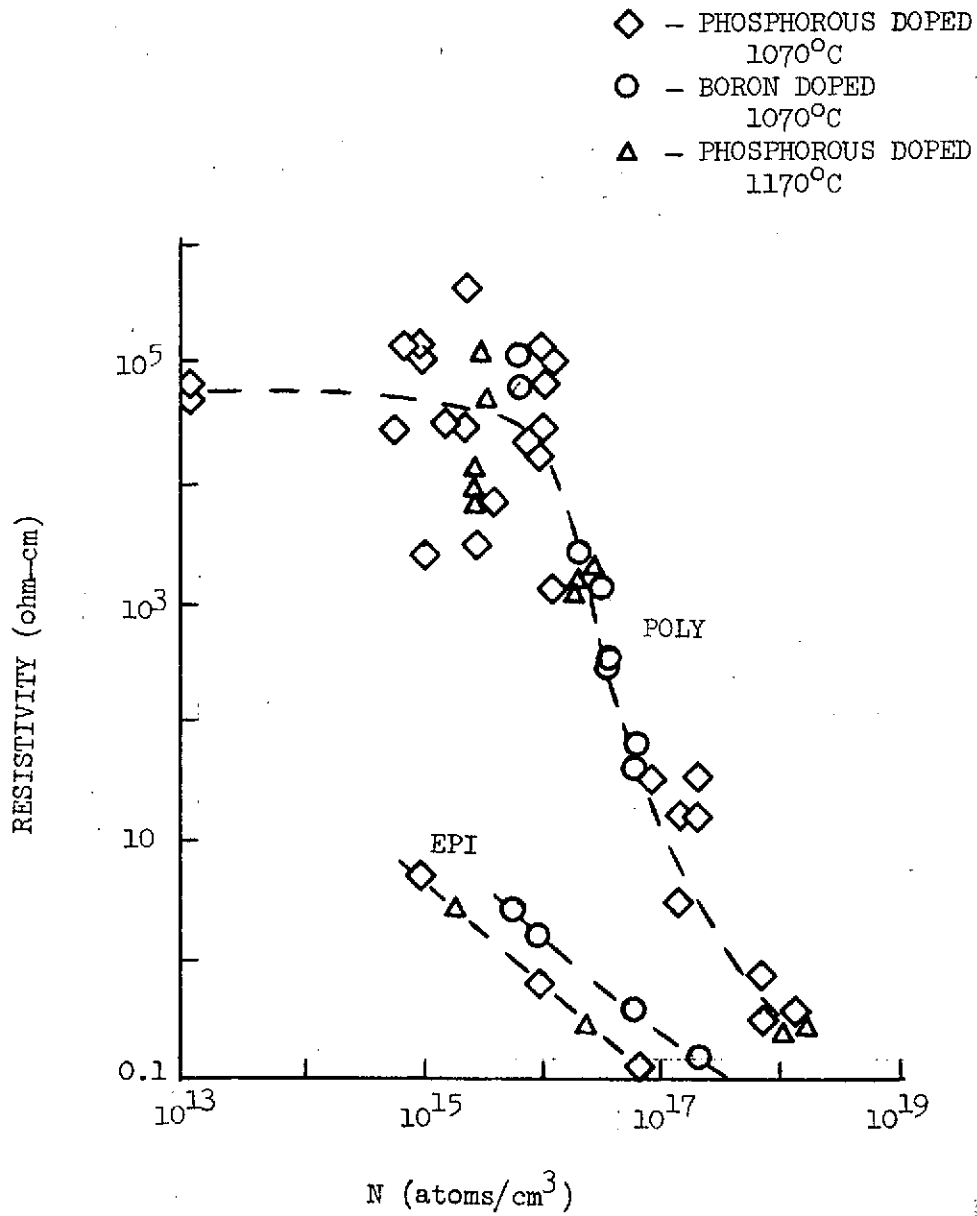


FIGURE 18. – COMPOSITE OF RESISTIVITY DATA, 10-MIN. DEPOSITIONS

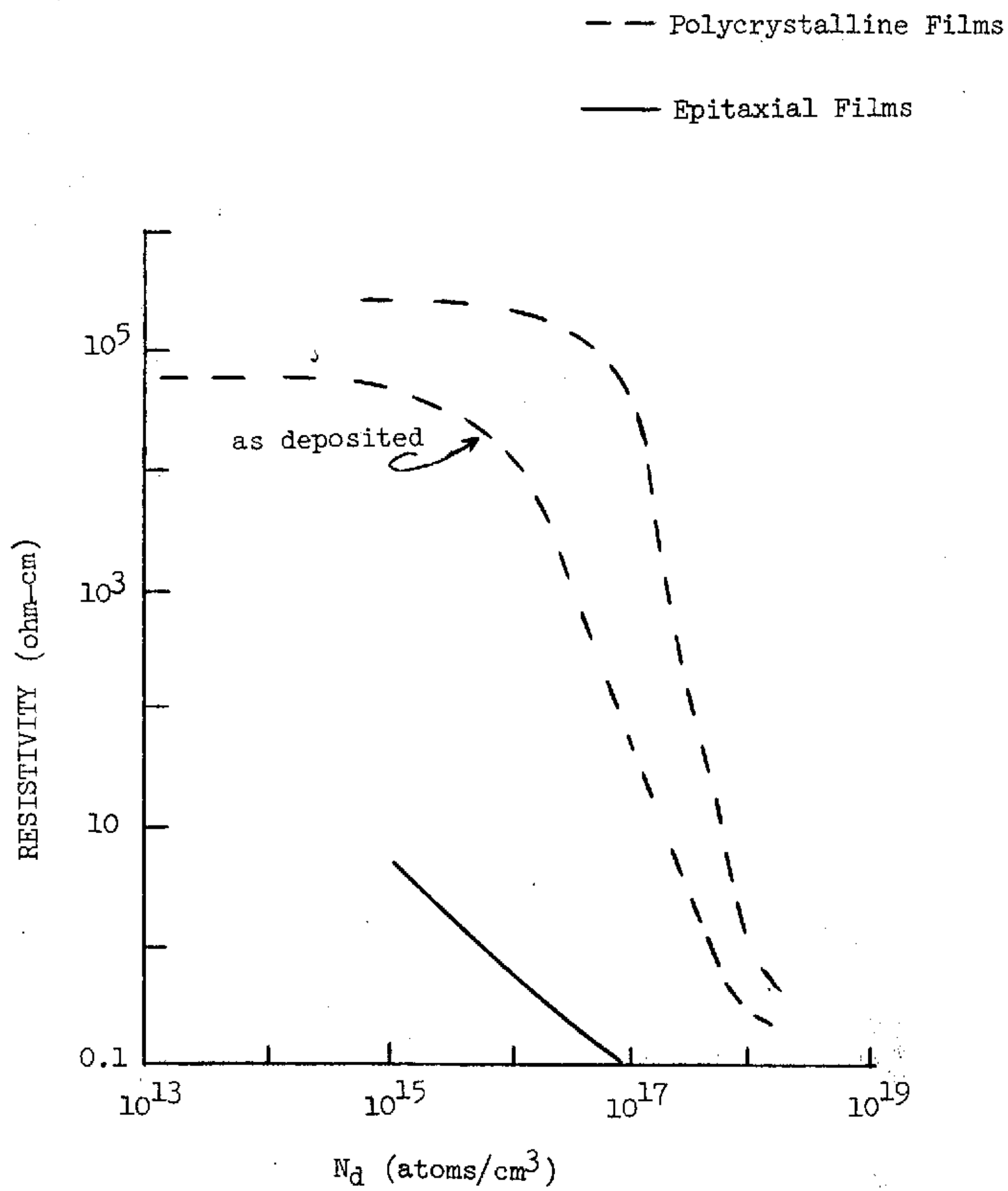


FIGURE 19. – RESISTIVITY OF SILICON FILMS BEFORE & AFTER ANNEAL

single crystal silicon oxidation have been well characterized (Ref. 65 is a good general reference on silicon oxidation) but investigation of oxidation of poly-crystalline silicon has received little previous attention (Ref. 41). In that paper (Ref. 41) the oxidation kinetics for polycrystalline silicon was very nearly the same as the single crystal when oxidized in dry oxygen. In the research performed for this dissertation, the oxidation kinetics also appeared the same for both structures when oxidation was performed in high temperature steam. Hence, it can be concluded that the grain boundaries do not have a significant effect on the oxidation rate.

It has also been shown that the resistivity of polycrystalline silicon films is thickness dependent where as the resistivity of co-deposited single crystal films is not thickness dependent. The thickness dependence is not observable after the crystalline grains in the films have reached a terminal dimension. That is, in films thinner than one micron, the resistivity increases and the grain size decreases as the vertical dimension is decreased.

# Chapter V

## Discussion

### Introduction

Single crystal films (epitaxial growth) grown in the same deposition system at the same time as the polycrystalline films exhibited the expected monotonic decreasing resistivity as doping gas concentration increased. The anomalous behavior of the resistivity of the polycrystalline silicon films is quite likely grain boundary related.

The difference in substrates for the two different films can be discounted as having a direct effect on the resistivity for two reasons. First, after the initial 1500A$^{o}$ of deposition, the surface is polycrystalline silicon, not silicon dioxide and second, a silicon dioxide film grown on an epitaxial silicon film does not produce a noticeable change in the resistivity, that is, the formation of a silicon-silicon dioxide interface does not cause a significant change in the resistivity of crystalline silicon. Of course, the presence of the amorphous silicon dioxide causes the formation of a polycrystalline instead of a single crystal film and, to that extent, the results are substrate dependent. The data, previously shown, on resistivity-vs-grain size

strongly indicates that the anomaly is not only caused by the grain boundaries, but is also grain size dependent. The polycrystalline films with the smaller grains (that is, the films less than one micron thick) had a greater resistivity than the films with larger grains. The thin epitaxial films grown at the same time, on the same susceptor, exhibited constant resistivity with respect to thickness.

Heat treatment, in an oxidizing atmosphere, had a stabilizing effect on the polycrystalline films. The minimum time for stabilization was less than fifteen minutes. Hence, what ever mechanism which produced the equilibrium resistivity did not require a high energy input. At 1100°C, fifteen minutes is sufficient to grow approximately 3000A° of silicon dioxide or in considering diffusion, provide a diffusion length of

$$2\sqrt{Dt} = 0.3 \ \mu m \tag{7}$$

where D = diffusion coefficient for phosphorous in single crystal silicon at 1100°C.

t = time at diffusion temperature

in single crystalline silicon.

# I. Model Development

## A. Application of Linear Circuit Theory

The equation for resistivity will now be examined and the components of the equation will be considered separately to see how the resistivity anomalies may occur.

The equation for the resistivity of a homogeneous semiconductor is:

$$\rho = \frac{1}{\sigma} = \frac{1}{e\ n_e\ \mu_e + e\ n_h \mu_h} \tag{8}$$

where

$\rho$ = resistivity in ohm-cm

$\sigma$ = conductivity, in (ohm-cm)$^{-1}$

$e$ = electron charge = $1.60 \times 10^{-19}$ coulomb

$\mu_e$ = mobility of an electron, in cm$^2$ volt$^{-1}$ sec$^{-1}$

$n_e$ = density of electronic charge carriers, in cm$^{-3}$

$\mu_h$ = mobility of a hole

$n_h$ = density of holes

In an intrinsic semiconductor, the only available charge carriers are produced by a broken bond in the crystal lattice such that a hole and an electron are simultaneously produced. Consequently, the density of holes and electrons are equal and the equation for resistivity is reduced to:

$$\rho = \frac{1}{e\ n_i(\mu_e + \mu_h)} \tag{9}$$

where $n_i$ = intrinsic carrier concentration

In bulk, single crystal, silicon at room temperature; (Ref. 4)

$n_i = 1.45 \times 10^{10}/cm^3$

$\mu_e = 1350\ cm^2$/volt sec (in intrinsic silicon)

$\mu_h = 480\ cm^2$/volt sec (in intrinsic silicon) ,

hence

$$\rho = 2.35 \times 10^5 \text{ ohm cm.} \tag{10}$$

In practice, silicon is usually intentionally alloyed with atoms that have either three or five valence electrons and which will enter the silicon lattice substitutionally. Since the tetrahedrally bonded silicon needs only four valence electrons, the alloyed, or dopant, atoms with five valence electrons will ionize, with a low activation energy, and produce an additional conduction electron without producing a conducting hole. Likewise, a dopant atom with three valence electrons can be negatively ionized to produce a conducting hole. The doping atoms, phosphorus and boron, used in this thesis ionize with activation energies of approximately 0.045 ev and experiment has shown that virtually all of the dopant

atoms are ionized at room temperature[4]. Hence, in a doped semiconductor the equation for resistivity reduces to:

$$\rho = \frac{1}{e\ N_d\ \mu_n} \tag{11}$$

if the dopant atoms have five valence electrons or

$$\rho = \frac{1}{e\ N_a\ \mu_h} \tag{12}$$

if the dopant atoms have three valence electrons

where $N_d$, $N_a$ = concentration of dopant atoms, if the concentration of one is much greater than the other.

The resistivity equation will have to be modified for a non-homogeneous material. If the semiconductor contains layers (Fig. 20), perpendicular to the direction of the electric field, which exhibit different carrier concentrations and different mobilities, and assuming no rectifying junctions, an apparent resistivity can be derived by considering:

$$R = \rho^{*}\ \ell/A \tag{13}$$

$$\rho^{*} = R\ A/\ell \tag{14}$$

But,

$$R = R_1 + R_2 + \ldots \tag{15}$$

$$R = \rho_1 \frac{\ell_1}{A} + \rho_2 \frac{\ell_2}{A} + \ldots \tag{16}$$

Hence,

$$\rho^* = \frac{1}{\ell} [\rho_1 \ell_1 + \rho_2 \ell_2 + \ldots] \tag{17}$$

or,

$$\rho^* = \frac{1}{\ell e} \left[\frac{\ell_1}{n_1 \mu_1} + \frac{\ell_2}{n_2 \mu_2} + \ldots\right] \tag{18}$$

where: $R$ = measured resistance of the sample, in ohms

$\rho^*$ = apparent resistivity, in ohm-cm

$\ell$ = length of sample, in cm

$A$ = cross sectional area of sample, in $cm^2$

$\ell_1(\ell_2)$ = length of first (second) layer, in cm

$n_1(n_2)$ = concentration of charge carriers in first (second) layer

$\mu_1(\mu_2)$ = mobility of charge carriers in first (second) layer

Another type of non homogeneous semiconductor can be modeled as having layers, parallel (Fig. 21) to the

electric field, with different carrier concentrations and mobilities. The apparent resistivity can be derived in a similar fashion as before.

$$\rho^* = R \frac{A}{\ell} \tag{19}$$

$$R = \frac{1}{\frac{1}{R_1} + \frac{1}{R_2} + \ldots} \tag{20}$$

For algebraic simplicity, assume only two conducting layers.

So,

$$R = \frac{R_1 R_2}{R_1 + R_2} \tag{21}$$

$$R = \frac{\ell \rho_1 \rho_2}{\rho_1 A_2 + \rho_2 A_1} \tag{22}$$

and,

$$\rho^* = \frac{\rho_1 \rho_2 A}{\rho_1 A_2 + \rho_2 A_1} \tag{23}$$

or,

$$\rho^* = \frac{A}{e} \frac{1}{(A_2 n_2 \mu_2 + A_1 n_1 \mu_1)} \tag{24}$$

where $A_1 (A_2)$ = cross sectional areas of layer one (two).

The third and last model of a non homogeneous material which will be considered is shown in Figure 22. In this model, type one material is surrounded by type two material. The type two material will be assumed to go from one face of the resistor to the other face. The apparent resistivity of this model can be derived by considering:

$$\rho^{*} = R \frac{A}{\ell} \tag{25}$$

$$R = \frac{R_a R_b}{R_a + R_b} \tag{26}$$

where:

$R_a$ = resistance of all the interlaced layers, in parallel

$R_b$ = resistance of all of the type two layers, in parallel, which go from one fact to the other face

From equation 16, we have the resistance for one of the parallel strips making up $R_a$ and the total resistance of $N$ such strips in parallel would be found by dividing by $N$.

$$R_a = \rho_1 \frac{\ell_1}{A_1} \frac{N_1}{N} + \rho_2 \frac{\ell_2}{A_1} \frac{N_2}{N} \tag{27}$$

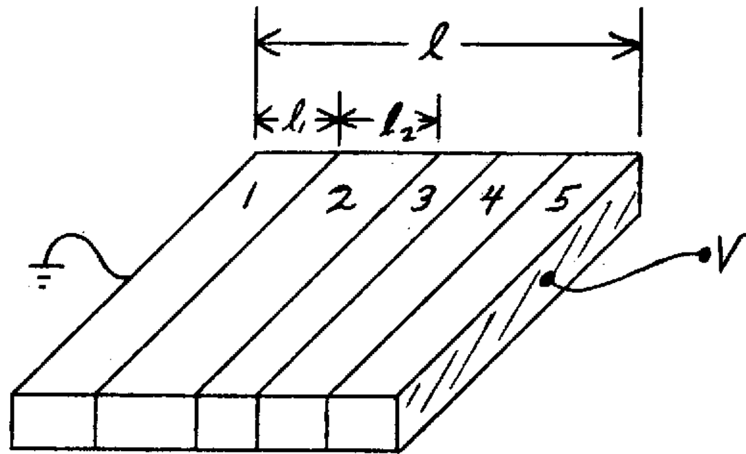


Figure 20.- Nonhomogeneous conductor- perpendicular layers.

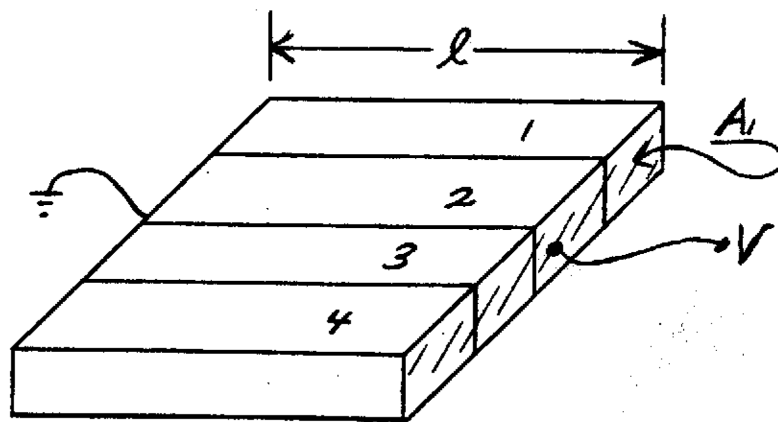


Figure 21.- Nonhomogeneous conductor- parallel layers.

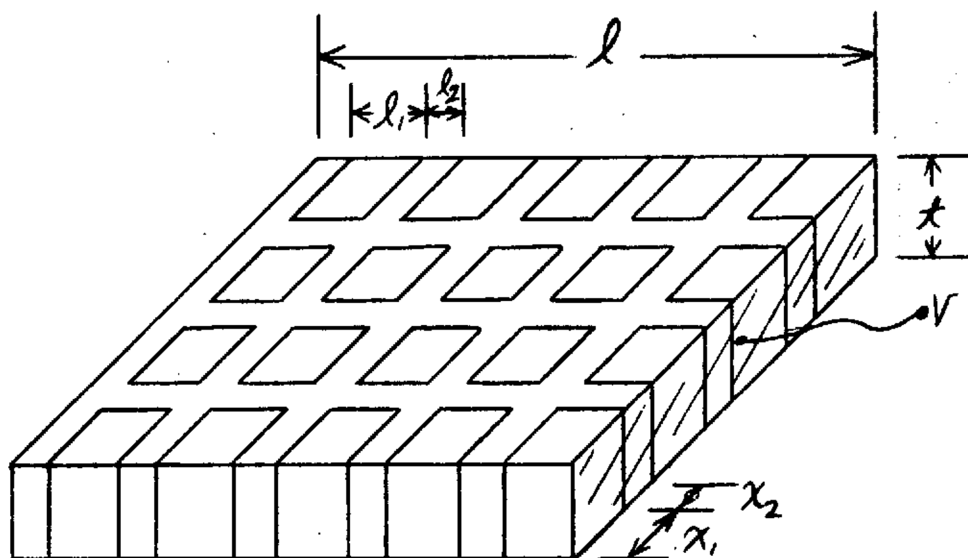


Figure 22.- Nonhomogeneous conductor- perpendicular and parallel layers.

where $N_1$ = number of segments of material one, in a single strip, which goes between the outer faces parallel to the electric field.

$N_2$ = number of segments of material two, in a single strip, which goes between the outer faces parallel to the electric field.

If $N$ is large then $N_1 \approx N_2$ and,

$$R_a = \frac{N_1}{N}\left(\rho_1 \frac{\ell_1}{A_1} + \rho_2 \frac{\ell_2}{A_1}\right) \tag{28}$$

A further simplification can be made if it is assumed that:

$$N = N_1$$

and

$x_1 = \ell_1$

$x_2 = \ell_2$, see Figure 22 for identification of X1 , X2

Then,

$$R_a = \frac{1}{t}\left(\rho_1 + \rho_2 \frac{\ell_2}{\ell_1}\right) \tag{29}$$

where $t$ = the thickness of the conducting material (see Figure 22).

The equation for $R_b$ is simply the resistance of one type two strip divided by $N$, hence:

$$R_b = \rho_2 \frac{\ell}{A_2 N} \tag{30}$$

or,

$$R_b = \rho_2 \frac{\ell}{Nt\ \ell_2} \tag{31}$$

The total resistance can now be calculated.

$$R = \frac{\left(\rho_1 + \rho_2 \frac{\ell_2}{\ell_1}\right) \frac{\rho_2\ \ell}{Nt\ \ell_2}}{\rho_1 + \rho_2 \left(\frac{\ell_2}{\ell_1} + \frac{\ell}{N\ell_2}\right)} \tag{32}$$

and,

$$\rho^* = \frac{\left(\rho_1 + \rho_2 \frac{\ell_2}{\ell_1}\right) \rho_2 \frac{\ell}{N\ell_2}}{\rho_1 + \rho_2 \left(\frac{\ell_2}{\ell_1} + \frac{\ell}{N\ell_2}\right)} \tag{33}$$

or,

$$\rho^* = \frac{(\ell_1 + \ell_2)}{e\ n_2\ \mu_2} \left[\frac{n_1\ \mu_1\ \ell_2 + n_2\ \mu_2\ \ell_1}{n_2\ \mu_2\ \ell_1\ \ell_2 + n_1\ \mu_1\ (\ell_2^2 + \ell_1\ \ell_2 + \ell_1^2)}\right] \tag{34}$$

A polycrystalline film may be modeled as shown in Figure 22, with the crystal grain representing the type one material and the grain boundary representing type two, if crystalline grains grow perpendicular to the substrate

and if the substrate is non-conducting. The poly-crystalline silicon films investigated in this thesis meet the criterion. Not only can it be assumed that once the nucleation growth stage is completed the films will continue to grow epitaxially upon the grains but photographs (Ref. 38, 46) of the cross section of a film also strongly indicates this epitaxial type growth. The substrate is certainly non conducting. Silicon dioxide has one of the highest resistivities known and should a pin hole occur in the oxide conduction still will not occur since the film and the substrate are opposite conductivity types. The crystalline grains are not square of course, but they do appear to be of nearly uniform size and show no radial size variation.

Quantitative values can be placed on some of the variables in equation 34 as follows:

$\mu_s$ = mobility of electrons in single crystal silicon

$\mu_s$ = (300 $cm^2$/volt sec, $N_D = 10^{18}/cm^3$

(1350 $cm^2$/volt sec, $N_D \leq 10^{15}/cm^3$

$\ell_s$ = average grain diameter ≈ 1 micrometer, if film thickness > 1 micrometer

$\ell_{gb}$ = width of grain boundary ≈ three atomic spaces (Ref. 67)

$\ell_{gb}$ = 10A°

The equation for resistivity can be written as

$$\rho^{*} = \frac{1}{eG}\left[\frac{10^{3}\ G + S}{G + 10^{3}\ S}\right] \tag{35}$$

where:

$e$ = electron charge = $1.6 \times 10^{-19}$ coulombs

$G = \mu_{gb}\ n_{gb}$

$S = \mu_{s}\ n_{s}$

Reasonable bounds can be placed, a priori, on the three remaining unknowns before the experimental data is examined.

The carrier concentration in the single crystal grains will equal the dopant concentration in the grains unless this concentration is very small. In that case, the thermally induced carriers will represent the lower carrier concentration. Hence,

$$1.4 \times 10^{10} \leq n_{s} \leq N_{d} \tag{36}$$

Neither $\mu_{gb}$ nor $n_{gb}$ can be vanishingly small or no conductivity could take place in the film. It can be assumed that due to structural disorder, mobility in the grain boundary will be less than in the crystalline grain. Hence,

$$0 < \mu_{gb} < \mu_{s} \tag{37}$$

Some distribution of dopant atoms between grain and grain boundary can be readily assumed but a quantitative value is not known. If the grain boundary region absorbed all dopant atoms, then $N_g$, the dopant atomic concentration in the grain boundary region would be much larger than $N_d$ because of the relative volumes.

It cannot be assumed that all dopant atoms which are deposited in the grain boundary will easily be ionized, hence, the range of grain boundary carrier concentration will be

$$0 < n_{gb} \leq \frac{V_f}{V_{gb}} N_d \tag{38}$$

$$0 < n_{gb} \leq 500\ N_d \tag{39}$$

where:

$V_f$ = volume of the film

$V_{gb}$ = total volume of grain boundary region.

The bounds on the unknowns will now be further limited by examining the resistivity equation (equation 35) with respect to the experimental data. The curve of the stabilized (annealed films) resistivity-vs-phosphorous doping level (Figure 10) will be used to obtain values of $\rho^*$ and $N_D$. The discussion will commence with the low doping level region and then extend into the more highly doped regions.

B. Application of Theory to Data - Low Doping Levels

Below a doping level of approximately $10^{16}$ phosphorous atoms per cubic centimeter the resistivity is essentially that of intrinsic single crystal silicon. This fact makes it enticing to assume that

$$S \approx \mu_i n_i \tag{40}$$

where:

$\mu_i$ = intrinsic single crystal silicon mobility

$n_i$ = intrinsic single crystal silicon carrier concentration

and that nearly all doping atoms reside in the grain boundaries when the film is in equilibrium (ie., after the heat treatment).

As stated previously, $G$ must be non zero or electrical conduction cannot occur. Since $N_g$ is assumed to be increasing with $N_d$ it should also be assumed that

$$G \propto N_d \tag{41}$$

Since $S$ is not expected to decrease with increasing $N_d$, it is necessary to use the set of $G$ and $S$, in equation 35, that will give a value of $\rho^*$ which is constant, within experimental accuracy, as $N_d$ increases. To obtain

this set of $G$ and $S$, a value of $S$, near the intrinsic value, was arbitrarily chosen and the corresponding value of $G$, for

$$\rho^* = 2.5 \times 10^5 \text{ ohm-cm}$$

was calculated from

$$G = \frac{10^3(1-4x10^{-14}S) + [10^6(1-4x10^{-14}S)^2 + 1.6x10^{-27}S]^{1/2}}{8x10^{-14}} \tag{42}$$

This calculated value of $G$ was then allowed to become

$$G' = \gamma G \tag{43}$$

$\gamma$, representing an increasing $N_d$, and for each increase a new value of resistivity was calculated with $G'$ replacing $G$ in equation 35. Figure 23 shows the sensitivity of the resistivity for the different values of $G$. Table XIX gives representative values of $G$ and $S$ for which the resistivity changes approximately 50% or less, as $\gamma$ is varied over

$$1 \leq \gamma \leq 1000 \tag{44}$$

and S is held constant.

Table XIX

Acceptable Values of G

| G | S | $\rho^*(\gamma = 10^3)$ |
|---|---|---|
| $3.1\times10^{12}$ | $2.52\times10^{13}$ | $2.21\times10^{5}$ |
| $9.16\times10^{11}$ | $2.57\times10^{13}$ | $2.34\times10^{5}$ |
| $3.37\times10^{11}$ | $2.70\times10^{13}$ | $2.28\times10^{5}$ |

Note that for the acceptable values of G, the values of S change only by a small percentage and are very close to the intrinsic value of

$$S = 1.96\times10^{13} \left(\frac{\text{carriers}}{\text{volt sec cm}}\right), \text{ electron carriers only}$$

or (45)

$$S = 2.65\times10^{13} \left(\frac{\text{carriers}}{\text{volt sec cm}}\right), \text{ hole and electron carriers} \tag{46}$$

The values of G given in Table XIX are physically viable if: (I.) A large percentage of dopant atoms are trapped in the grain boundary in such state, such as all five valence electrons satisfying a covalent bond in the disordered grain boundary, that they are not easily ionized and/or (II.) The charge carrier mobility is

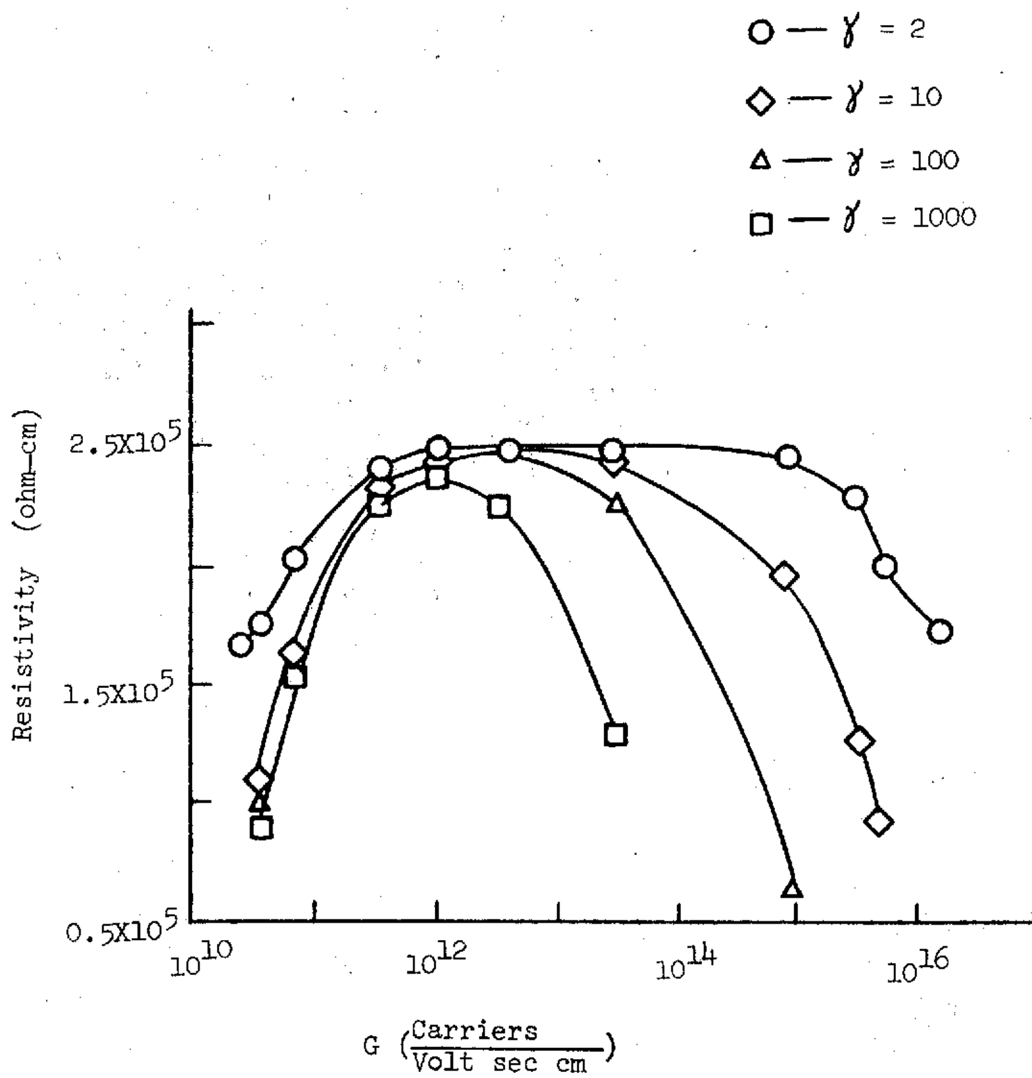


FIGURE 23. – SENSITIVITY OF APPARENT RESISTIVITY

considerably lower in the grain boundary region than in the crystalline region. These proposals are feasible and they will each be examined below.

The total number of dopant atoms tied up in the grain boundaries would be related to the film dopant concentration by

$$N_g \approx 500\ N_d \tag{47}$$

Hence, in the doping range of

$$10^{13} < N_d < 10^{16} \text{ atoms/cm}^3 \tag{48}$$

the grain boundary range would be

$$5 \times 10^{15} < N_g < 5 \times 10^{18} \text{ atoms/cm}^3 \tag{49}$$

If the charge carrier mobility in the grain boundary region was arbitrarily assumed to be approximately one percent of the single crystal value, then

$$N_{gb} \approx \begin{cases} 10^{10} \text{ carrier/cm}^3 \text{ at } N_d = 10^{13} \text{ atoms/cm}^3 \\ 10^{13} \text{ carriers/cm}^3 \text{ at } N_d = 10^{16} \text{ atoms/cm}^3 \end{cases} \tag{50}$$

Hence, the majority of dopant atoms in the grain boundary region would have to be in sites which render them electrically inactive.

The disorder of the grain boundary would provide other than tetrahedral atomic sites as can be accounted for in the existance interfacial energy. The number of extra bonds in the grain boundary can be estimated by considering the interfacial energy and the energy to create one bond.

The surface energy of silicon has been given as

$$\varepsilon_s = 1230 \text{ ergs/cm}^2 \text{ (Ref. 68)} \quad . \tag{51}$$

If the grain boundary energy can be estimated by

$$\varepsilon_g \approx \frac{1}{3}\,\varepsilon_s \quad \text{(Ref. 69)} \tag{52}$$

then, the density of extra bonds is

$$N_B \simeq \frac{1}{3}\,\varepsilon_s\, A_{gb}\, \frac{1}{1.1 \text{ ev/bond}} \tag{53}$$

$$N_B = 5 \times 10^{18} \text{ extra bonds/cm}^3 \tag{54}$$

where

$$A_{gb} = \text{area of grain boundaries/cm}^3$$
$$A_{gb} = 2\text{x}10^4 \text{ cm}^2\text{/cm}^3 \tag{55}$$

This value for extra bonds in the silicon interface is in excellent agreement with the upper limit of equation 49.

C. Discussion of General Conditions

As the doping concentration increases a knee in the curve is reached and the resistivity rapidly drops as the doping concentration continues to increase. Finally another break in the curve is reached where the rate of resistivity decrease drops to nearly an inverse function of $N_d$.

Obviously, the crystalline grain contributes to the conduction equation at the higher doping levels. Before applying the derived equations to the data obtained for the higher doping levels, some of the apparent boundary conditions will be discussed.

1. Maximum Grain Boundary Solubility

The grain boundary cannot continue to absorb the dopant atoms indefinitely because of solid solubility limits. The solid solubility limit of phosphorus in single crystalline silicon is

$$N_{d(max)} \approx 4 \times 10^{20} \text{ atoms/cm}^3 . \qquad (56)$$

No data exists for the solid solubility level of phosphorus in silicon grain boundaries, but McLean[67] uses a value

of 1/3 for the ratio of solute to host atoms in metal grain boundaries. Hence,

$$N_{g(max)} \approx 1.7 \times 10^{22} \text{ atoms/cm}^3 \quad . \tag{57}$$

Which means that it would be possible for the grain boundaries to absorb all dopant atoms as long as the film doping concentration was

$$N_d \leq N_{g(max)} \frac{2\ell_2}{\ell_1} \tag{58}$$

$$N_d \leq 3 \times 10^{19} \text{ atoms/cm}^3 \quad . \tag{59}$$

The doping concentrations used in this thesis were at least an order of magnitude less than this limit.

2. Minimum Value of Resistivity

No minimum value of resistivity was found, hence, a model must provide for a decreasing resistivity for doping levels greater than used in the experiments. The main point here is that the value of $G$ cannot terminate too quickly. For example, when

$$N_d = 1.5 \times 10^{18} \text{ atoms/cm}^3 \tag{60}$$

the measured value of resistivity is

$$\rho^{*} = 0.5 \text{ ohm cm} \tag{61}$$

and the minimum permissible value of $G'$ is

$$G' = 1.25 \times 10^{16} \frac{\text{carriers}}{\text{volt sec cm}} \tag{62}$$

The value of $G$ used in these conclusions produce a $G'$ at this doping level which is much larger than $1.25 \times 10^{16}$.

3. Concentration of Dopant Atoms

As discussed earlier, the weighted sum of $n_g$ and $n_s$ need not equal $N_d$, but

$$\frac{2\ell_2}{\ell_1} N_g + N_s \equiv N_d \tag{63}$$

and

$$N_s = n_s \ . \tag{64}$$

These conditions have been and will be observed.

D. Application of Theory to Data - High Doping Levels

The ability of the values of $G$ obtained from the high resistivity data to fit the experimental data in the decreasing resistivity regions was examined by calculating the values of $S$, from

$$S = \frac{G'(e\rho^{*}G' - 10^{3})}{(1 - 10^{3}\ e\rho^{*}G')} \tag{65}$$

needed to satisfy the experimentally determined $\rho^{*}$ for

$$G' = \gamma G \tag{66}$$

$$\gamma = \frac{N_d}{10^{13}} \tag{67}$$

The value of $S$ is, of course, directly related to $n_s$ and if $n_s$ is much greater than the intrinsic level, $S$ is also directly related to $N_s$. The calculated values of $G$ obtained from equation 42 and shown in Figure 23 were used as a parameter in equation 65. Only the three values of $G$ given in Table XIX produced physically tenderable values of $S$ (that is $S$ must be greater than the intrinsic value and must never decrease with increasing $N_d$). Figure 24 shows the rise in $S$ as a function of $N_d$ for

$$G = 9.2 \times 10^{13} \frac{\text{carriers}}{\text{volt sec cm}} \quad . \tag{68}$$

The curve is very similar for the other two values of $G$. Hence, the value of $G$ given in Table XIX are viable in both the high and low doping regions.

II. Thin Films

The ratio of the concentration of dopant atoms in the grain to the concentration in the grain boundary, that is, the segregation coefficient, constantly increases with $N_d$ once past the doping level of approximately $10^{16}$ atoms/cm$^3$. However, at any given doping level, the segregation coefficient was essentially zero until

$$N_g \approx 5 \times 10^{18} \text{ atoms/cm}^3 \quad . \tag{69}$$

With a grain size of one micron that value of $N_g$ occurred at

$$N_d \approx 10^{16} \text{ atoms/cm}^3 \quad . \tag{70}$$

As the grain size decreases, this critical value will occur at higher values as:

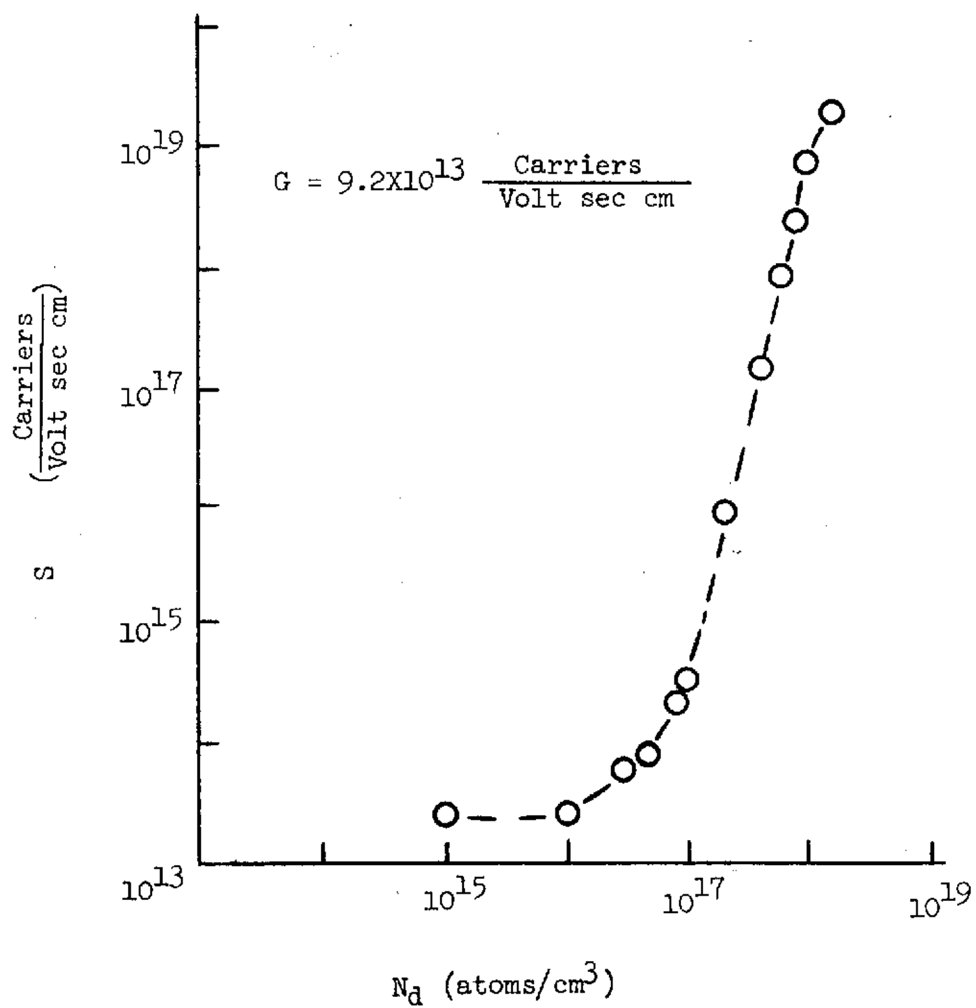


FIGURE 24. — S vs. DOPANT LEVEL

$$N_d \text{ (crit)} \approx 5 \times 10^{18} \left(\frac{2\ell_2}{\ell_1}\right) \text{ atoms/cm}^3 \quad . \tag{71}$$

Due to the steep descent of resistivity with respect to doping level, a small increase of the knee of the curve produces large effects on the resistivity at the higher doping levels.

The data shown in Figure 8 shows the resistivity increasing by a factor of approximately 40 as the thickness of a polycrystalline film, doped at $10^{18}$ atoms/cm$^3$, decreases to 0.5 μm. If, for lack of a better functional relationship, the grain size is assumed to be linear with thickness for vertical dimensions between 1500A$^o$ and one micron, the critical doping level at 0.5 μm will be

$$N_d \text{ (crit)} \approx 2 \times 10^{16} \text{ atoms/cm}^3 \quad . \tag{72}$$

Consequentially, the resistivity of the thinner film would be expected to increase to a value of the thicker films which were deposited with one half of the total doping concentration. That is,

$$\rho^*(t = 0.5 \text{ μm}, N_d = 10^{18}) = \rho^*(t > 1 \text{ μm}, N_d = 5\text{x}10^{17}) \tag{73}$$

The data in Figure 10 shows the resistivity increasing by a factor of 16 as $N_d$ drops from $10^{18}$ atoms/cm$^3$ to

$5x10^{17}$ atoms/$cm^3$.

III. Resistivity of As Deposited Films

The resistivity of the as deposited films was lower than the annealed films and it had considerably more scatter. The lower resistivity can be explained by assuming that many dopant atoms are temporarily trapped in the crystalline grain since the film is growing faster than a dopant atoms can diffuse through it. The heat treatment after deposition allows the dopant atoms to seek their minimum energy positions which is assumed to be the grain boundary region.

IV. Consideration of Alternate Models

A. Charge Carrier Traps

One possible suggestion for the shape of the resistivity-vs-doping level curve could be the existence of charge carrier (rather than dopant atoms) traps in the interface. This model is discounted because of the following reasons:

(a) Heat treatment, annealing, would be expected to remove traps, not increase them. Hence, the resistivity should have either been unaffected by heat treatment or it should have decreased.

(b) In the doping region tested, both n and p doped films behaved in a similar manner. Hence, the traps would have to be effective for both type carriers.

B. Oxide Barriers

Another alternate model would be to assume that the oxidizing, annealing, step formed a high resistivity barrier between highly conducting grains. The reasons for not considering this model further are:

(a) The oxide is etched off of the surface before electrical measurements are made. It would be expected that the oxide barrier would also be removed and that additional oxidation would further increase the resistivity.

(b) The coincidence of the barriers producing an apparent resistivity equal to that of intrinsic silicon is not to be expected.

C. Hydrogen in the Grain Boundaries

The last model considered is that of hydrogen being trapped in the grain boundaries and causing resistivity anomalies. This model was not extended because:

(a) If the hydrogen was trapped as atoms, it would be easily ionized. This would add conduction electrons to the n-type material and remove a

conducting hole from the p-type material. In the experiments, both n and p type films behaved similarly.

(b) If hydrogen was trapped as molecules, as it may be, they might coalase and form pores. These pores would restrict the film's conducting path and raise the resistivity. However, the size of the pores would not be expected to be doping level dependent.

# Chapter VI

## Summary

Polycrystalline silicon films have been grown on thermally oxidized silicon wafers by the pyrolytic decomposition of silane. The resistivity of these films was measured as a function of dopant concentration, film thickness, and post deposition heat treatment.

The resistivity of the films was independent of doping concentration but widely scattered in the lightly doped region. Heat treatment in an oxidizing atmosphere removed the scatter in the data such that the measured resistivity was approximately that of intrinsic silicon. The resistivity decreased rapidly as the doping concentration became greater than $10^{17}$ atoms/cm$^3$ in the heat treated films. Heat treatment did not produce a noticeable change in the resistivity of epitaxial films.

The resistivity of the polycrystal films was independent of thicknesses above one micron. Below one micron the resistivity increased rapidly as the films became thinner.

It was assumed that the grain boundaries trap the dopant atoms. As the doping concentration increases, the segregation coefficient of the grain boundaries decreases and more dopant atoms can contribute to conduction in the grains.

Linear circuit theory was used to develop a model of the polycrystalline film in which the crystalline grains and the grain boundary regions are each represented as separate conductors. The apparent resistivity was then given by

$$\rho^* = \frac{1}{eG} \left[ \frac{10^3 G + S}{G + 10^3 S} \right] \qquad (74)$$

where:

$e$ = electron charge

$G = \mu_{bg} n_{gb}$

$S = \mu_s n_s$

$\mu_{gb}(\mu_s)$ = mobility of a charge carrier in the grain boundary (grain)

$n_{gb}(n_s)$ = concentration of charge carriers in the grain boundary (grain)

Due to the measured value of resistivity in the lower doped region the value of $S$ was assumed to be approximately equal to that of intrinsic silicon. The value of

$$G = 9 \times 10^{11} \frac{\text{carriers}}{\text{volt sec cm}} \qquad (75)$$

and

$$S = 2.57 \times 10^{13} \frac{\text{carriers}}{\text{volt sec cm}} \qquad (76)$$

produced the most acceptable results in the low doping region for they did not produce a large variation in the resistivity if it was assumed that $G$ increased linearily with $N_d$ and $S$ remained constant until the doping level was reached where the measured resistivity began to decrease.

The values of $S$ were calculated in the highly doped region by using the measured value of $\rho^*$ and assuming that $G'$ continued to increase as

$$G' = \gamma G \tag{77}$$

$$\gamma = \frac{N_d}{10^{13}} \tag{78}$$

These calculated values of $S$ showed a sharply increasing doping concentration in the crystalline grains as $N_d$ increased past $10^{17}$ atoms/cm$^3$.

Alternate models based on charge carrier trapping, oxide barrier formation, and hydrogen entrapment were considered and rejected.

## References


1. Fundamentals of Silicon Integrated Device Technology, Volume I, R. M. Burger and R. P. Donovan, Editor, Prentice-Hall, Inc., Englewood Cliffs, N. J. (1967).

2. D. C. Gupta: "Improved Methods of Depositing Vapor-Phase Homoepitaxial Silicon". Solid State Technology, 14, 33 (October 1971).

3. J. D. Filby and S. Nielsen: British Journal of Applied Physics, 18, 1357 (1967).

4. A. S. Grove, Physics and Technology of Semiconductor Devices, John Wiley and Sons, Inc., New York (1967).

5. W. Shockley: Electrons and Holes in Semiconductors, D. Van Nostrand Co. Inc., New York (1950).

6. Integrated Silicon Device Technology, Technical Documentary Report No. ASD-TDR-63-316, vol. 1-16, Contract No. AF33(657)-10340, Research Triangle Institute, Durham, N. C.

7. R. M. Warner, Editor: Integrated Circuits-Design Principles and Fabrication, McGraw-Hill Book Co. New York, 1965.

8. J. C. Sarace, R. E. Kerwin, D. L. Klein, and R. Edwards: "Method-Nitride-Oxide-Silicon Field-Effect Transistors, with Self-Aligned Gates". Solid-State Electronics, 11, 653 (1968).

9. F. Faggin and T. Klein, "Silicon Gate Technology." Solid-State Electronics, 13, 1125 (1970).

10. W. F. Kosonocky and J. E. Carnes, "Charge-Coupled Digital Circuits." IEEE Journal of Solid-State Circuits, SC-6, 314 (1971).

11. C. K. Kim and E. H. Snow; P-Channel Charge-Coupled Devices with Resistive Gate Structure." Applied Physics Letters, 20, 514 (1972).

12. M. H. White, D. R. Lampe, F. C. Blaha, and I. A. Mark; "Charge-Coupled Device (CCD) Imaging at Low Light Levels." Paper Presented at the International Electron Devices Meeting, Washington, D. C., December 6, 1972.

13. H. C. Lin, J. L. Halsor, and P. J. Hayes: "Shielded Silicon Gate Complementary MOS Integrated Circuit." IEEE Transactions on Electron Devices, ED-19, 1199 (1972).

14. G. L. Schnable, A. F. McKelvey, and J. A. Hastings: "A Chemical Technique for Preparing Oxide-Isolated Silicon Wafers for Microcircuits." Electrochemical Technology, 4, 57 (1966).

15. D. A. Maxwell, R. H. Beeson, and D. F. Allison: "The Minimization of Parasitics in Integrated Circuits by Dielectric Isolation." IEEE Transactions on Electron Devices, ED-12, 20 (1965).

16. D. Adler, "Theory Gives Shape to Amorphous Materials", Electronics, p. 61 (September 28, 1970).

17. M. H. Cohen; "Theory of Amorphous Semiconductors." Physics Today, p. 26 (May 1971).

18. F. M. Collins; "Vacuum Evaporated Silicon Films" Transactions of the Eighth National Vacuum Symposium, 2, p. 899 (1962).

19. H. Richter and O. Fiirst; Z. Naturforsch, 6a, p. 38 (1951).

20. G. H. Hass; "Studies on the Structure and Behavior of Thin Evaporated Films of Silver, Aluminum, Silicon, and Germanium" U. S. Army Report 1026 Project 8-23-02-002, Dec. 18, 1947, Washington, D. C.

21. A. H. Clark: Electrical and Optical Properties of Amorphous Germanium." Physical Review, 154, p. 750 (1967).

22. M. H. Brodsky, R. S. Title, K. Weiser, and G. D. Pettit; "Structural, Optical, and Electrical Properties of Amorphous Silicon Films." Physical Review B, 1, p. 2632 (1970).

23. A. J. Mountvala and G. Abowitz: "Textural Characteristics and Electrical Properties of Vacuum Evaporated Silicon Films." Vacuum, 15, p. 359 (1965).

24. P. A. Walley; "Electrical Conduction in Amorphous Silicon of Germanium", Chin Solid Films, 2, p. 327 (1968).

25. Y. Onuma and K. Sekiya; "Piezoresistive Properties of Polycrystalline Silicon Thin Films". Japanese Journal of Applied Physics, 11, 20 (1972).

26. H. Y. Kumagai, J. M. Thompson, and G. Krauss; "Properties and Structure of Thin Silicon Films Sputtered on Fused Quartz Substrates." Transactions of the Metallurgical Society of AIME, 236, p. 295 (1966).

27. P. G. Le Comber, A. Madon, and W. E. Spear; "Electronic Transport and State Distribution in Amorphous Si Films." Journal of Non-Crystalline Solids, 11, 219 (1972).

28. R. C. Chittick, J. H. Alexander; and H. F. Sterling; The Preparation and Properties of Amorphous Silicon." Journal of the Electrochemical Society, 116, p. 77 (1969).

29. J. C. Krwin; "Resistivity of Bulk Silicon and of Diffused Layers in Silicon." The Bell System Technical Journal, 41, 387 (1962).

30. M. Braunstein, R. R. Henderson, and R. I. Braunstein; Moving Mask Growth of Single-Crystal Silicon Films on Amorphous Quartz Substrates". Applied Physics Letters, 12, 66 (1968).

31. J. D. Filby and S. Nielsen; "Progress Toward Single Crystal Silicon Films on Amorphous Substrates". Journal of the Electrochemical Society, 112, 957 (1965).

32. J. D. Filby, and S. Nielsen; "Selected Area Deposition of Single Crystal Silicon on Amorphous Quartz". Journal of the Electrochemical Society, 113, 1091 (1966).

33. Y. Kataoka; "Some Properties of Evaporated Silicon Films", Journal of the Physical Society of Japan, 17, 967 (1962).

34. F. D. King, J. Shewchun, D. A. Thompson, H. D. Barber, and W. A. Pieczonka; Polycrystalline Silicon Resistors for Integrated Circuits." Solid State Electronics, 16, 701 (1973).

35. J. D. Heaps, O. N. Tufte, and A. Nassbaum: "Vapor-Deposited Polycrystalline Silicon Solar Cells." IRE Transactions on Electron Devices, ED-8, 560 (1961).

36. "The Polysilicon Insulated Gate Field-Effect Transistor." IEEE Transactions on Electron Devices, ED-13, 290 (1966).

37. E. Sirtl and H. Seiter: "Vapor-Deposited Micro-crystalline Silicon." Journal of the Electro-chemical Society, 113, 506 (1966).

38. A. L. Fripp; "Deposition and Evaluation of Silicon Films Formed by Pyrolytic Decomposition of Silane on Oxidized Silicon Single Crystals." Master of Materials Science Thesis, University of Virginia, 1969.

39. A. L. Fripp, R. L. Stermer, and A. Catlin; "Structure of Silicon Films Deposited on Oxidized Silicon Wafers." Journal of the Electrochemical Society, 117, 1569 (1970).

40. J. D. Joseph and T. I. Kamins; "Resistivity of Chemically Deposited Polycrystalline-Silicon Films" Solid-State Electronics, 15, 355 (1972).

41. T. I. Kamins and E. L. MacKenna; "Thermal Oxidation of Polycrystalline Silicon Films." Metallurgical Transactions, 2, 2292 (1971).

42. T. I. Kamins and T. R. Cass; "Structure of Chemically Deposited Polycrystalline-Silicon Films." Submitted for publication in Thin Solid Films.

43. M. E. Cowher and T. O. Sedgwick; "Chemical Vapor Deposited Polycrystalline Silicon." Journal of the Electrochemical Society 119, 1565 (1972).

44. G. L. Pearson and J. Bardeen; "Electrical Properties of Pure Silicon and Silicon Alloys Containing Boron and Phosphorous." Physical Review, 75, 865 (1949).

45. K. E. Bean, H. P. Hentzschel, and D. Colman; "Thermal and Electrical Anisotropy of Polycrystalline Silicon." Journal of Applied Physics, 40, 2358 (1969).

46. T. I. Kamins, J. Manoliu, and R. N. Tucker; "Diffusion of Impurities in Polycrystalline Silicon." Journal of Applied Physics, 43, 83 (1972).

47. K. E. Bean, H. P. Hentzschel, and D. Colman; "Thermal and Electrical Properties of Polycrystalline Silicon in the Dielectric Isolation Process." Semiconductor Silicon, R. R. Haberecht and E. C. Kern, editors; p. 747, Electrochemical Society, Inc., New York (1969).

48. Precision Gas Products, Inc., Catalogue, p. 8017.

49. T. I. Kamins, "Hall Mobility in Chemically Deposited Polycrystalline Silicon." Journal of Applied Physics, 42, 4357 (1971).

50. F. C. Eversteyn and B. H. Put; "Influence of $A_5H_3$, $PH_3$, and $B_2H_6$ on the Growth Rate and Resistivity of Polycrystalline Silicon Films Deposited from a $S_iH_4$-$H_2$ Mixture." Journal of the Electrochemical Society, 120, 106 (1973).

51. W. Shockley; "Dislocations and Edge States in the Diamond Crystal Structure". Physical Review, 91, 228 (1953).

52. W. T. Read, Jr.; "Theory of Dislocation in Germanium," Philosophical Magazine, 45, 775 (1954).

53. W. T. Read, Jr.; "Statistics of the Occupation of Dislocation Acceptor Centers", Philosophical Magazine, 45, 1119 (1954).

54. R. H. Glaengen and A. G. Jordan; "The Electrical Properties of Dislocations in Silicon - I, The Effects on Carrier Lifetime." Solid-State Electronics, 12, 247 (1969).

55. R. H. Glaenger and A. G. Jordan; "The Electrical Properties of Dislocations in Silicon - II, The Effects on Conductivity." Solid-State Electronics, 12, 259 (1969).

56. J. P. Hirth and J. Lothe; Theory of Dislocations, McGraw-Hill Book Co., New York (1968).

57. R. L. Ramey and W. D. McLennon; "Charge-Carrier Mobility in Polycrystalline Semiconducting Films Based on Bulk Single-Crystal Theory". Journal of Applied Physics, 38, 3491 (1967).

58. R. L. Ramey, W. A. Jesser, and T. L. Bowers; "Dislocation and Surface Scattering in Polycrystalline Germanium Films." Journal of Applied Physics, 41, 5304 (1970).

59. W. E. Taylor, N. H. Odell, and H. Y. Fon; "Grain Boundary Barriers in Germanium." Physical Review, 88, 867 (1952).

60. R. K. Mueller; "Current Flow Across Grain Boundaries in n-Type Germanium, I". Journal of Applied Physics, 32, 635 (1961).

61. R. K. Mueller; "Current Flow Across Grain Boundaries in n-Type Germanium, II". Journal of Applied Physics, 32, 640 (1961).

62. Y. Matukura; "Properties of Grain Boundaries in Silicon." Journal of the Physical Society of Japan, 16, 842 (1961).

63. Y. Matukura; "Grain Boundary States in Silicon and Germanium". Japanese Journal of Applied Physics, 2, 91 (1963).

64. F. M. Smits; "Measurement of Sheet Resistivities with the Form Point Probe." Bell System Technical Journal, 37, 711 (1958).

65. B. E. Deal; The Oxidation of Silicon in Dry Oxygen, Wet Oxygen, and Steam". Journal of the Electrochemical Society, 110, 529 (1963).

66. R. F. Donovan, "Oxidation" in Fundamentals of Silicon Integrated Device Technology, Edited by R. M. Burger and R. P. Donovan, Prentice-Hall, Inc., Englewood Cliffs, N. J. 1967.

67. D. McLean, Grain Boundaries in Metals, Oxford University Press, London, 1957. p. 42.

68. R. J. Jaccodine, "Surface Energy of Germanium and Silicon", Journal of the Electrochemical Society", 110, 524 (1963).

69. R. A. Swalin; Thermodynamics of Solids, John Wiley and Sons, Inc., New York 1962.

THE FOLLOWING PAGES ARE DUPLICATES OF ILLUSTRATIONS APPEARING ELSEWHERE IN THIS REPORT. THEY HAVE BEEN REPRODUCED HERE BY A DIFFERENT METHOD TO PROVIDE BETTER DETAIL